Ocean Engineering 262 (2022) 112250

Contents lists available at ScienceDirect

Ocean Engineering

journal homepage: www.elsevier.com/locate/oceaneng

A probabilistic approach for Dynamic Positioning capability and operability predictions

Francesco Mauro [a,c,*], Radoslav Nabergoj [b]

[a] The Maritime Safety Research Centre, Department of Naval Architecture, Ocean and Marine Engineering (NAOME), University of Strathclyde, 100 Montrose St., Glasgow, G4 0LZ, Scotland, UK
[b] NASDIS PDS d.o.o., Industrijska Cesta, 2e, Izola, 6310, Slovenia
[c] Department of Maritime and Transport Technology, Faculty of Mechanical, Maritime and Materials Engineering, Delft University of Technology, 17 Leeghwaterstraat, Delft, 2628 CA, the Netherlands

ARTICLE INFO

Keywords:
Dynamic positioning
Operability
Offshore vessels
Joint environmental conditions
Quasi-Monte Carlo method

ABSTRACT

Determining Dynamic Positioning capability for an offshore vessel is mandatory to identify the environmental forces the system can counteract, together with the operability in a specific operational area of interest. Conventional predictions evaluate the capability as a maximum sustainable wind speed at a predefined encounter angle for a given wind–wave correlation, not reflecting the effective wind and waves occurrence at the site. In this respect, a step forward is provided by the scatter diagram approach, allowing the evaluation of operability in a specific sea area, using a simplified method to predict wind speed from wave parameters. Here, using known wind–waves joint distributions for the long-term environmental conditions further improves the scatter diagram approach, assessing the operability of a Dynamic Positioning system through a Quasi-Monte Carlo sampling of the joint distribution. Analysing the results of the Quasi-Monte Carlo process, it is possible to obtain a site-specific capability plot, allowing the identification of critical wind speeds in a way that is familiar to operators in the offshore industry. The application of this novel method in the case of quasi-static calculations both to a reference supply vessel and a pipe-lay vessel shows the flexibility of the proposed approach for site-specific Dynamic Positioning capability predictions.

1. Introduction

The performance evaluation of any Dynamic Positioning (DP) system is a mandatory step for the design process of an offshore unit (Balchen et al., 1976), as the DP system is one of the fundamental installations equipping ships working in an offshore environment (Kumar, 2020). Such an analysis allows determining the maximum environmental forces that the DP system can counteract, using all the thruster devices mounted on-board and accounting for system failures (Aalberts et al., 1995). The conventional approach for the study of DP system capabilities aims to determine the maximum sustainable wind speed the unit can face in prescribed environmental conditions (ABS, 2014; DNV, 2021), obtaining the so-called DP capability plots (IMCA, 2000) or regulatory indices assessing DP performances (DNV, 2011; BV, 2021; LR, 2021). This target and its representation can be achieved with different prediction methodologies, implying the adoption of quasi-static calculations (Aalberts et al., 1995; Wang et al., 2018) or time-domain simulations (Smogeli et al., 2013; Mauro and Gaudiano, 2018; Martelli et al., 2022).

Regardless of the methodology adopted to assess DP capability, all the conventional methods imply the modelling of environmental loads (Aydin et al., 2022) separating the effects of wind, waves and current, assuming wind–wave correlations (general or site-specific) and keeping a constant current speed (IMCA, 2000; DNV, 2021). Such a deterministic and semi-empirical approach does not account for all the possible combinations between significant wave height H_s and wave peak period T_p that may statistically occur in a specific geographic area but limits the analysis to a predetermined set of few combinations derived from the recommended or calculated wind–wave correlations. An alternative vision of the problem has been recently given by the "scatter diagram approach" (Mauro and Prpić-Oršić, 2020), where the predictions cover all the $H_s - T_p$ combinations provided by a scatter diagram for specific locations. In such a way, the DP system is no more evaluated by a capability plot but through the yearly operability of the vessel in the selected sea area. This method improves the wave environment modelling but still has limiting approximations to associate the wind speed V_w with the varying wave parameters. Therefore, the method can be considered as a quasi-probabilistic assessment.

* Corresponding author.
E-mail addresses: F.Mauro@tudelft.nl (F. Mauro), radoslav.nabergoj@nasdispds.com (R. Nabergoj).

https://doi.org/10.1016/j.oceaneng.2022.112250
Received 29 June 2022; Received in revised form 29 July 2022; Accepted 7 August 2022
Available online 17 August 2022
0029-8018/© 2022 The Author(s). Published by Elsevier Ltd. This is an open access article under the CC BY license (http://creativecommons.org/licenses/by/4.0/).

Table 1
Methods for DP analyses according to different environmental modelling.

#	Method	Environmental modelling				Output	
		Wind	Wave	Current	Directions	Capability	Operability
1	Deterministic DP capability	Wind–wave correlation		Fixed	Collinear	✓	–
2	Site-specific DP capability	Site-specific wind–wave correlation		Fixed or varying with env. conditions	Collinear or site-specific	✓	–
3	Scatter diagram approach	P–M correlation	Scatter diagram	Fixed or varying with env. conditions	Collinear or site-specific	–	✓
4	Probabilistic approach	Trivariate site-specific joint distribution		Fixed or varying with env. conditions	Collinear or site-specific	✓	✓

The approximated evaluation of wind speed V_w in the "scatter diagram approach" is a limitation to its full applicability for dynamic positioning performance predictions in a specific sea environment. Furthermore, the "scatter diagram approach" is entirely decoupled from the standard capability calculations, forcing the end users to perform conventional analyses besides the quasi-probabilistic approach to visualise the traditional DP capability. The present work fills this gap and presents a new "fully probabilistic" methodology to assess site specific DP capability and operability predictions by improving the wind–wave correlation modelling of the "scatter diagram approach".

The development and testing of a novel and original prediction process based on a Monte Carlo (MC) integration allow evaluating the DP operability sampling the environmental conditions from site-specific joint distributions for wind and wave characteristics (Johannessen et al., 2001). However, the DP analysis with the base MC process on two reference vessels in two different sea areas, where environment statistics is available (Li et al., 2013), highlights the necessity to improve the sampling process by implementing an enhanced Quasi-Monte Carlo (QMC) method (Niederreiter, 1992) to reduce the variability of the solution and decrease the total amount of calculations necessary to determine the vessel's DP operability with a given accuracy.

Furthermore, besides operability, the enhanced "fully probabilistic" method allows deriving a site-specific capability plot, filling the second weakness of the "scatter diagram approach", visualising the maximum sustainable wind speed at each vessel heading χ and inheriting the probabilistic nature of the novel DP performance assessment. This last aspect increases the feasibility of the new method, providing an additional output which is a state-of-the-art diagram easily interpretable for offshore operators.

The novel contributions provided by the "fully probabilistic" DP analysis cover the following main focal points:

- Probabilistic modelling of site-specific environmental conditions.
- Operability calculation for a specific operative site through an MC integration process.
- Optimisation of the MC process employing an enhanced QMC algorithm.
- Evaluation of DP capability directly from operability calculations.

The present work also allows to clearly distinguish between the available processes to evaluate the capability and operability of a DP system, providing a comprehensive overview and comparison of the methods. The results of the reference cases highlight the importance of enhanced modelling of the combined wind–wave characteristics for a more realistic operability prediction of the DP system. The comparison with standard deterministic and standard site-specific DP analyses is self-evident. Table 1 summarises the main differences between inputs and outputs of the existing processes, highlighting the completeness of the newly proposed "fully probabilistic" approach compared to other procedures.

The paper has the following structure: Section 2 presents the reference vessels and the considered sea areas that will be employed through all the calculation presented in this work. The standard quasi-static approach is reviewed in Section 3 to explain the background of the adopted thrust allocation algorithm for equating the environmental loads and the applied external forces.

In Section 4 the hypotheses of the methods #1 to #3 in Table 1 are reviewed together with the corresponding environmental conditions used for DP assessment. The necessity of an enhanced modelling of long-term environmental conditions is discussed in Section 5 by presenting both bivariate and trivariate joint distributions of environmental parameters.

Section 6 deals with the fundamentals of the newly developed DP prediction method #4 (see Table 1) based on Montecarlo and Quasi-Montecarlo samplings. This novel method is physically well grounded and can be suitably used to supply both the DP operability evaluation on the scatter diagram statistics. The way to recover the capability plot from the samplings is detailed in Section 7, where an original vision of the standard DP capability plot in terms of probabilistic safety is introduced for the first time. Final remarks and conclusions are given in Sections 8 and 9, respectively.

2. Reference vessels and sea areas

The novel procedure for the probabilistic site-specific DP analysis is here applied on two reference vessels: one OSV unit and a PLCV one. These two vessels have been selected due to the availability of information on the thruster's size and their layout but also because the environmental loads are available from model experiments. As the developed methodology concerns site-specific calculations, use is made of two reference areas where detailed environmental statistics are available in literature. Hereafter, the vessels and the selected geographic areas are further described.

2.1. Reference OSV and PLCV

For sake of brevity, the two reference vessels will be referred through the text as *Vessel-1* and *Vessel-2*, see Table 2 for their main characteristics. *Vessel-1* is an example of OSV vessel, which is equipped with two azimuth thrusters and three tunnel ones, two on the bow and one on the stern. The configuration of the thrusters is symmetric and reflects a standard layout for OSVs. On the other hand, *Vessel-2* is a PLCV vessel equipped with six azimuth thrusters. The vessel presents a peculiarity compared to the previous layout, as the foremost thruster T1 is not located on the ships centreline, resulting in an asymmetrical thruster configuration. Moreover, the vessel is equipped with a cantilevered tower for J-lay operations located on the vessels side. Table 3 reports the thruster sizes and their locations for both vessels using the reference system of Fig. 1, together with the magnitude of the pipe loads applied to *Vessel-2*. Environmental loads coefficients for the two reference vessels are available from model experiments. Table 3 reports also the interaction areas between the azimuth thrusters, showing the main interaction angle τ_{int} and the amplitude of the interaction area δ. Due to the clustering of thrusters on the bow, *Vessel#2* presents two interaction areas for the bow devices, stern devices have only one as T6 is located at a different depth than T4 and T5.

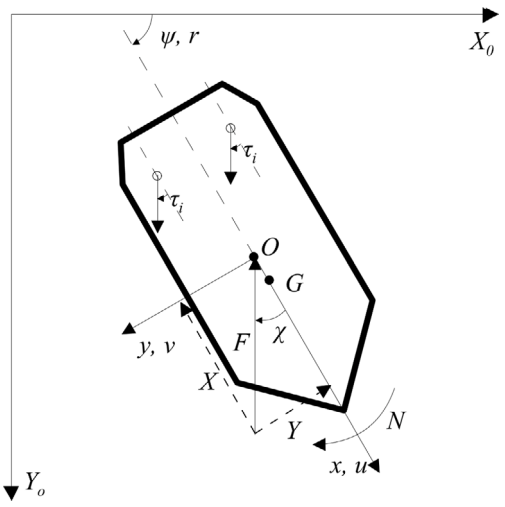

Fig. 1. Reference system for DP calculations.

Table 2
Main characteristics of reference vessels.

		Vessel-1	*Vessel-2*	Unit
Length between perpendiculars	L_{PP}	55.0	197.6	m
Length overall	L_{OA}	60.0	205.4	m
Maximum breadth	B	13.3	48.0	m
Operative draught	T	3.8	7.5	m
Volume	∇	2085.0	11747.6	m^3
Lateral exposed wind area	A_L	517.9	6100.0	m^2
Transversal exposed wind area	A_T	156.4	3300.0	m^2

2.2. Reference sea areas

This study aims at the determination of a site-specific DP capability prediction. Therefore, to test the procedure, use has been made of two reference geographic sea areas where joint probability distributions representative for V_w, H_s and T_p is available from the literature (Li et al., 2013). The two sites are representative of one buoy located in the Atlantic Ocean near Cabo Silleiro and the other in the North Sea near Norway's shore.

For brevity, the first sea area is named *Site A* and the second one *Site B*. Fig. 2 shows the scatter diagrams of the two reference sea-areas (normalised on 1000 wave realisations according to the Global Wave Statistics (Hogben et al., 1986)). A more detailed description of the joint environmental data of the two sea areas will follow in the dedicated sections.

3. Quasi-static Dynamic Positioning calculations

An exhaustive and detailed analysis of a DP system requires the execution of time-domain simulations, considering both vessel dynamics and the control system. Models for DP simulations generally employ 3 DOF dynamic equations derived from manoeuvring theory under vessel low-speed assumptions. With reference to system in Fig. 1, motion equations for a vessel with mass m and inertia I_z have the following form:

$$\begin{cases} m\left[\dot{u} - vr - x_G r^2 - y_G \dot{r}\right] &= X(t) \\ m\left[\dot{v} + ur - y_G r^2 + x_G \dot{r}\right] &= Y(t) \\ I_z \dot{r} + m\left[x_G(\dot{v} + ur) - y_G(\dot{u} - vr)\right] &= N(t) \end{cases} \quad (1)$$

where x_G, y_G are the centre of gravity coordinates. Variables u, v and r are the surge, sway and yaw velocities, respectively, while X, Y and N are external forces and moments acting on the vessel, including the thruster forces derived by the control system.

DP time-domain simulations require considerable computational effort and need the availability and knowledge of all the data necessary to set up both the hydrodynamic and controller models. An alternative and less computational demanding approach is the implementation of a quasi-static DP calculation. Even though this alternative neglects the dynamic effects or only accounts for them with an empirical correction on external loads, the quasi-static method allows the investigation of multiple environmental conditions in a reasonably short amount of time. Therefore, such a method is more suitable to study alternative allocation methods and vessel operability prediction without excluding future extension to the time-domain approach.

The quasi-static DP problem, neglecting vessel dynamics, requires the resolution of the forces and moment equilibrium on the horizontal plane. Therefore, adopting the same reference system of Fig. 1, the following equations system needs to be solved:

$$\begin{cases} \sum_{i=1}^{N_T} X_{T_i} &= X_{tot} \\ \sum_{i=1}^{N_T} Y_{T_i} &= Y_{tot} \\ \sum_{i=1}^{N_T} \left(Y_{T_i} x_{T_i} - X_{T_i} y_{T_i}\right) &= N_{tot} \end{cases} \quad (2)$$

where X_T and Y_T are the thrust components in x and y directions delivered by the N_T on-board actuators, located at x_T and y_T coordinates. The right-hand terms of system (2) represent the environmental and external loads. The latter allows the simulation of additional forces and moments acting on the vessel, like mooring lines or pipeline tensioning. The resolution of the quasi-static problem requires solving system (2), assuming the thrust components as unknowns.

3.1. Thrust allocation algorithm

The total number of unknowns in system (2) is $N_{TT} + 2N_{ST}$, with N_{TT} being the number of fixed tunnel thrusters and N_{ST} being the number of steerable ones. Thus, except for the unrealistic case of one steerable and one fixed thrusters, the problem admits infinite feasible solutions, having the equilibrium system only three equations. Therefore, a suitable resolution algorithm has to be used to properly evaluate the distribution and orientation of the thrust among the actuators. This study uses a non-linear optimisation method (Mauro and Nabergoj, 2016), employing a non-linear objective function representative of the sum of absorbed power by each thruster:

$$\min(z) = \sum_{i=1}^{N_T = N_{TT} + N_{ST}} \left(\sqrt{X_{T_i}^2 + Y_{T_i}^2}\right)^{\frac{2}{3}} \quad (3)$$

The algorithm can handle as unknowns both the thrusters thrust components or the thrust intensity and its orientation (Mauro et al., 2021). Here, the selection of thrust components as unknowns allows keeping linear the main optimisation equality constraints, i.e. the equilibrium equations of system (2). Besides, additional inequality constraints have to ensure that the actuators deliver thrust up to their maximum limits:

$$\sqrt{X_{T_i}^2 + Y_{T_i}^2} \leq F_{T_{max_i}} \text{ for } i = 1, \ldots, N_T \quad (4)$$

Such constraints-set is non-linear. Thus, non-linear programming or constraints linearisation is suitable to solve the problem. Having the two reference ships' interaction zones between azimuth thrusters (see Table 3), the additional constraints are not sufficient to solve the optimisation problem. More advanced thrust allocation algorithms automatically evaluate the thruster–thruster interaction effect (Prpić-Oršić and Valčić, 2020; Mauro and Nabergoj, 2016; Arditti et al., 2019), autonomously giving preference to thruster orientations with lower power demand (Mauro and Nabergoj, 2015a; Arditti et al., 2015). However, such algorithms rarely apply to standard quasi-static predictions, and a conventional allocation method is more suitable to present the novel probabilistic procedure. With the adopted thrust allocation strategy, additional implementation of forbidden zones can model the thruster–thruster interaction between azimuth devices, forcing the thrust outside the interaction area by automatically adding additional equality constraints when needed (Mauro, 2022).

Table 3
Thrusters characteristics, thrusters interaction zones and external loads of reference vessels.

Vessel-1					*Vessel-2*				
Thruster ID	x_T (m)	y_T (m)	D (m)	P_S (kW)	Thruster ID	x_T (m)	y_T (m)	D (m)	P_S (kW)
T1 (*tunnel*)	22.5	0.0	1.25	603	T1 (*azimuth*)	84.4	−6.0	3.60	4500
T2 (*tunnel*)	20.0	0.0	1.25	603	T2 (*azimuth*)	65.2	−14.0	3.60	4500
T3 (*azimuth*)	−27.5	−3.0	2.60	2210	T3 (*azimuth*)	65.2	14.0	3.60	4500
T4 (*azimuth*)	−27.5	3.0	2.60	2210	T4 (*azimuth*)	−89.2	−14.0	3.60	4500
T5 (*tunnel*)	−22.5	0.0	1.25	603	T5 (*azimuth*)	−89.2	14.0	3.60	4500
					T6 (*azimuth*)	−98.8	0.0	3.60	4500
Thruster ID	First inter. zone		Second inter. zone		Thruster ID	First inter. zone		Second inter. zone	
	τ_{int} (deg)	δ (deg)	τ_{int} (deg)	δ (deg)		τ_{int} (deg)	δ (deg)	τ_{int} (deg)	δ (deg)
T1	–	–	–	–	T1	135.0	24.4	−149.0	27.4
T2	–	–	–	–	T2	59.0	27.4	90.0	22.8
T3	−90.0	30.0	–	–	T3	−45.0	24.4	−90.0	22.8
T4	90.0	30.0	–	–	T4	–	–	90.0	22.8
T5	–	–	–	–	T5	–	–	−90.0	22.8
					T6	–	–	–	–
External load ID	x_{ext} (m)	y_{ext} (m)	X_{ext} (kN)	Y_{ext} (kN)	External load ID	x_{ext} (m)	y_{ext} (m)	X_{ext} (kN)	Y_{ext} (kN)
					L1 (*Pipe line*)	−22.0	27.5	−1471.0	0.0

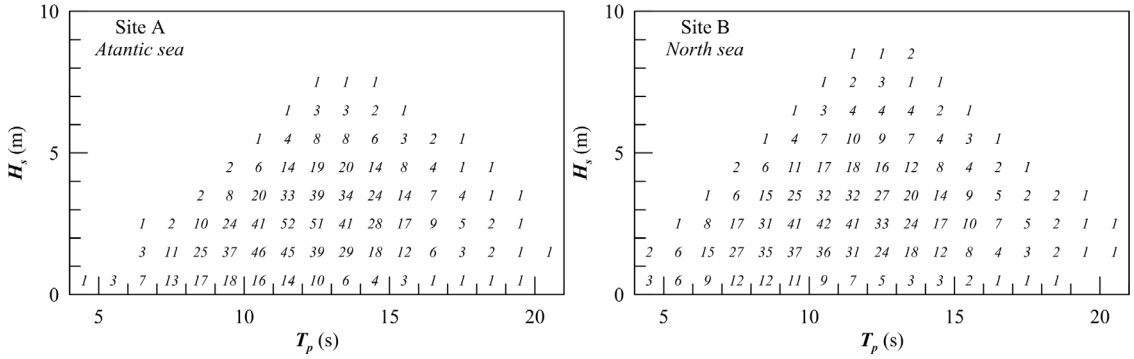

Fig. 2. Wave scatter diagrams for *Site A* and *Site B*.

3.2. Environmental and external loads

A relevant aspect of a quasi-static DP prediction is evaluating environmental loads acting on the unit. Besides, particular vessel types as PLV may be subjected to additional external loads like pipeline tensioning. A general decomposition of the right-hand loads of equations system (2) is as follows:

$$\begin{cases} X_{tot} = X_{wind} + X_{wave} + X_{curr} + X_{ext} \\ Y_{tot} = Y_{wind} + Y_{wave} + Y_{curr} + Y_{ext} \\ N_{tot} = N_{wind} + N_{wave} + N_{curr} + N_{ext} \end{cases} \tag{5}$$

In the case of pipeline tensioning, the external load is assumed constant with the vessel heading. On the contrary, the estimate of environmental loads is necessary for all encounter angles the unit will face during stationing. The use of non-dimensional coefficients for the environmental loads characterisation grants more flexibility for the reproduction of multiple environmental conditions. This approach is straightforward for wind loads, where the total forces and moment can be expressed by means of non-dimensional load coefficients with the following expressions:

$$\begin{cases} X_{wind} = \frac{1}{2}\rho_{air} A_F V_w^2 C_{X_W}(\chi) \\ Y_{wind} = \frac{1}{2}\rho_{air} A_L V_w^2 C_{Y_W}(\chi) \\ N_{wind} = \frac{1}{2}\rho_{air} A_L L_{OA} V_w^2 C_{N_W}(\chi) \end{cases} \tag{6}$$

where A_F and A_L are the frontal and lateral areas of the unit superstructures, L_{OA} is the overall length, V_w the mean wind speed and ρ_{air} the air density and χ the heading angle.

Current loads can be described with expression analogue to (6), where superstructure areas are substituted by wetted surface S. Reference is made to current speed V_C and water density for salt water ρ_w:

$$\begin{cases} X_{curr} = \frac{1}{2}\rho_w S V_C^2 C_{X_C}(\chi) \\ Y_{curr} = \frac{1}{2}\rho_w S V_C^2 C_{Y_C}(\chi) \\ N_{curr} = \frac{1}{2}\rho_w S L_{OA} V_C^2 C_{N_C}(\chi) \end{cases} \tag{7}$$

Wave loads are described by means of mean drift forces, representative of an irregular and usually long-crested sea for specific couples of H_s and T_p. Mean drift forces can be measured through dedicated model scale experiments or derived from the quadratic transfer functions (QTF) calculated by diffraction theory. Modelling the irregular sea environment with a spectrum it results:

$$\begin{aligned} X_{waves} &= \rho_w g \nabla^{\frac{1}{3}} \int_0^\infty C_{X_w}(\chi,\omega) S_\zeta(\omega)\,\mathrm{d}\omega \\ Y_{waves} &= \rho_w g \nabla^{\frac{1}{3}} \int_0^\infty C_{Y_w}(\chi,\omega) S_\zeta(\omega)\,\mathrm{d}\omega \\ N_{waves} &= \rho_w g \nabla^{\frac{2}{3}} \int_0^\infty C_{N_w}(\chi,\omega) S_\zeta(\omega)\,\mathrm{d}\omega \end{aligned} \tag{8}$$

where ∇ is the vessel volume of displacement, g the acceleration of gravity and S_ζ is the wave amplitude spectrum expressed as a function of circular wave frequency ω.

The simplified quasi-static DP calculations lead to the overestimation of the final station keeping ability of a vessel. It is possible to decrease this overestimation by adding a dynamic allowance to environmental loads, approximatively accounting for dynamic effects. The execution of time domain simulations on the same vessel allows a possible estimation of the dynamic allowance. However, without performing time-domain calculations, use can be made of guidelines given by regulations. In the present study, a dynamic allowance coefficient CA_{dyn}=1.25 is used to represent such allowances (DNV, 2021).

Table 4
Standard wind–wave correlations according to IMCA (2000) and DNV (2021).

IMCA			DNV		
V_w (m/s)	H_s (m)	T_p (s)	V_w (m/s)	H_s (m)	T_p (s)
0.0	0.0	–	0.0	0.0	–
2.5	1.28	5.30	1.5	0.1	3.5
5.0	1.78	6.26	3.4	0.4	4.5
7.5	2.44	7.32	5.4	0.8	5.5
10.0	3.21	8.41	7.9	1.3	6.5
12.5	4.09	9.49	10.7	2.1	7.5
15.0	5.07	10.56	13.8	3.1	8.5
17.5	6.12	11.61	17.1	4.2	9.0
20.0	7.26	12.64	20.7	5.7	10.0
22.5	8.47	13.65	24.4	7.4	10.5
25.0	9.75	14.65	28.4	9.5	11.5
27.5	11.09	15.62	32.6	12.1	12.0
30.0	12.50	16.58			
32.5	13.97	17.53			
35.0	15.49	18.46			

According to classification societies rules, it is possible to combine the environmental loads in different ways, e.g. by changing their directions or their relative contributions. Different ways of combining the simultaneous action of environmental loads and definition of reference environmental conditions leads to different kinds of quasi-static DP analyses. This problem will be investigated in the following section.

4. Environmental conditions in Dynamic Positioning analyses

A quasi-static approach in predicting DP capabilities allows performing several analyses, depending on the environmental conditions modelling. Conventional methods employ fixed combinations of wind speed and wave parameters through a deterministic relationship (wind–wave correlation). However, long-term environmental data improve the prediction reliability for site-specific calculations. Any more detailed probabilistic definition of the combined wind–wave environment requires a substantial change in the calculation process suitable to evaluate the effectiveness of a DP system.

The present section describes the commonly used environmental models for combined wind–wave action, defining the associated standard and more advanced DP analyses.

4.1. Wind–wave correlation

The most common and simple way to model the combined action of wind and waves is the use of a wind–wave correlation, providing a unique deterministic relationship between H_s, T_p and V_w. Even tough the relationship between wave parameters and wind speed changes with the operating location of the vessel, classification societies (DNV, 2021) and operators associations (IMCA, 2000) suggest the adoption of reference values reported in Table 4.

Another possibility is to derive the wind–wave correlation from an irregular wave spectrum formulation as, for example, the Pierson–Moskowitz (P–M) one, solving the following system:

$$\begin{cases} H_s &= \frac{2}{g}\sqrt{\frac{\alpha}{\beta}}V_w^2 \\ T_p &= 1.4049\frac{2\pi}{g\sqrt[4]{\pi\beta}}V_w \end{cases} \tag{9}$$

where α and β for the standard PM spectrum are two constants equal to 0.0081 and 0.74, respectively.

It is also possible to determine wind–wave correlations for site-specific environmental conditions (DNV, 2021). In such a case, wind–wave correlations are expressed through simplified models obtained from a direct comparison of cumulative density functions (CDF) of marginal distributions of V_w, H_s and T_p. Such an approximation generates triplets $V_w - H_s - T_p$ corresponding to the same occurrence in the given CDF analysis. That represents a simplified characterisation of a sea state, applicable when joint statistics of environmental variables are not available. Therefore, for DP applications, a site-specific wind–wave correlation offers environmental modelling with the same logical structure as the standard correlations already described, just adding specificity for the sea area of interest. Then, the adoption of site-specific wind–wave correlation does not change the evaluation process needed to assess DP capability with standard correlations.

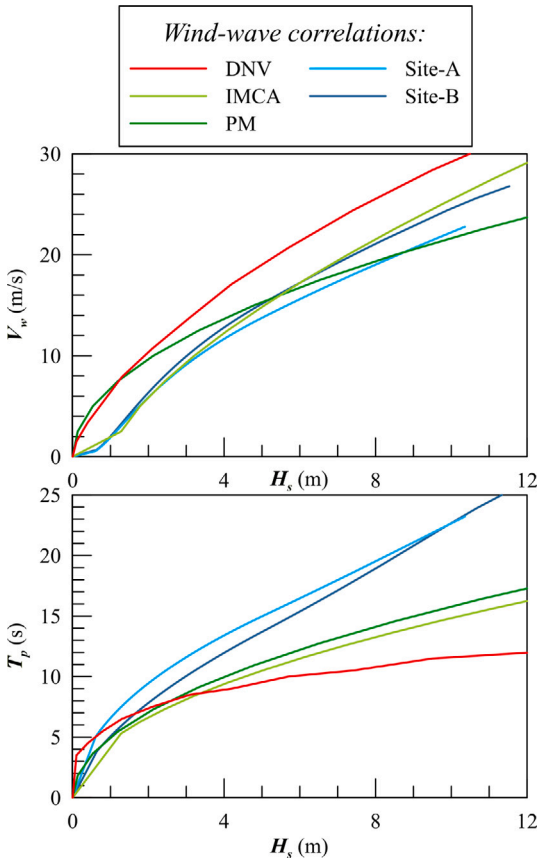

Fig. 3. DNV, IMCA, PM and site-specific (Site A and Site B) wind–wave correlations in $H_s - V_w$ plane (*top*) and $H_s - T_p$ (*bottom*).

Fig. 3 shows the comparison between conventional wind–wave correlations and those specific for Site A and Site B. All the correlations identify alternative triplets $V_w - H_s - T_p$ for the modelled environment.

Besides wind and wave loads, also current loads have to be taken into account. Regulations consider the current speed constant (except for DNV suggestions for low wind speeds) and all the environmental loads simultaneously acting on the vessel with the same encounter angle. The adoption of such kind of environment leads to the determination of the DP system capability through consecutive quasi-static calculations.

The representation of DP capability predictions can follow several standards, but all of them are different versions of the so-called Capability plot. This diagram represents the maximum sustainable wind speed $V_{W_{max}}$ the DP system can face, using the on-board thrust devices, at each encounter angle χ. Fig. 4 shows the capability plots obtained on the two reference vessels using the DNV, the IMCA and the Pierson–Moskowitz wind–wave correlations together with site-specific ones, with V_c=0.75 m/s for all cases and considering all the on-board actuators running. The capability plots indicate that the adoption of alternative wind–wave correlations influences the resulting DP capability prediction. The differences depend on the vessel type and actuators power. As site-specific correlations are defined up to the maximum

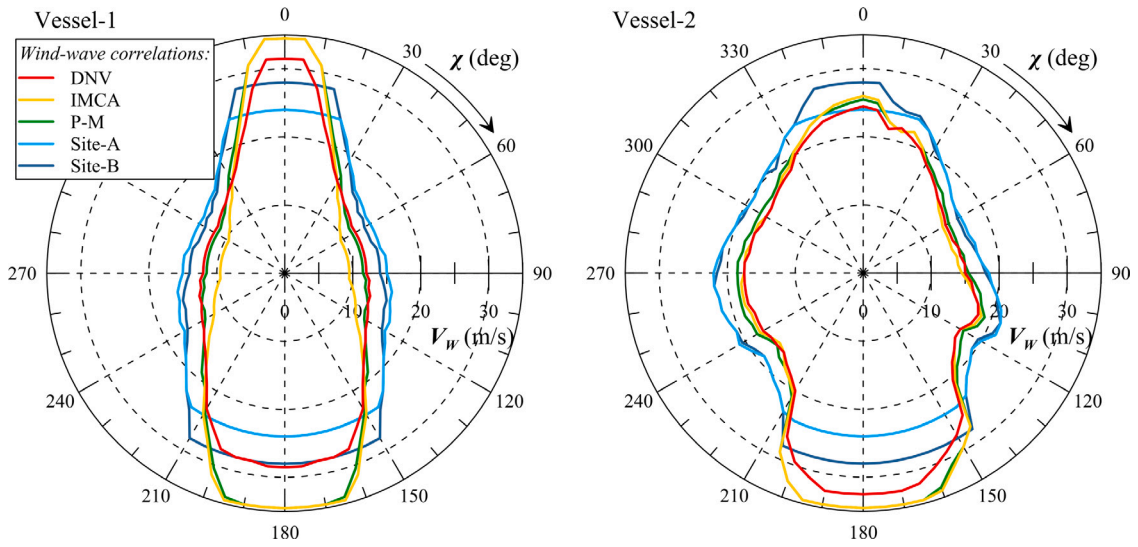

Fig. 4. DP capability plots according to IMCA, DNV, Pierson–Moskowitz (PM) and site-specific (Site A and Site B) wind–wave correlations for *Vessel-1* (*left*) and *Vessel-2* (*right*).

wind detected in the sea area, the associated capability plots are saturated at that specific limit, resulting in an apparent lower capability for head and stern directions.

The site-specific correlations give the highest $V_{W_{max}}$ between all the tested options, both for *Vessel-1* and *Vessel-2*. Even tough the correlations for Site A and Site B are different (see Fig. 3), the maximum capability limits do not differ too much, especially for *Vessel-2*. Within standard correlations, for *Vessel-1* the resulting capability plots with DNV and Pierson–Moskowitz wind–wave correlations show a higher capability for beam directions (approx. 4 kn spreading). The capability of *Vessel-2* is less influenced by the wind–wave correlation, but differences still remain for beam weather directions (approx. 2 kn spreading). For head and stern directions the DNV correlation gives lower capabilities compared to the other two also because of the lower maximum V_w value provided by the regulation.

These differences are due to the specific environmental conditions (i.e. the unique combinations of H_s, T_p and V_w), which differ for all the considered wind–wave correlations.

4.2. Scatter diagram approach

An alternative method to a deterministic wind–wave correlation is the adoption of the quasi-probabilistic scatter diagram approach (Mauro and Prpić-Oršić, 2020). This approach allows having a more comprehensive and complete overview of the DP system performances in a specific sea area. Instead of performing deterministic DP capability plot predictions, the scatter diagram approach allows the execution of DP calculations for each combination of H_s and T_p of the operational area. Calculations can be carried out for each heading χ, evaluating whether the DP system is able or not to keep the vessel in position with the resulting sea environment.

A wave scatter diagram gives statistical data for H_s and T_p only. Therefore, the corresponding wind speed remains unknown and should be derived using specific assumptions. The methodology described by Mauro and Prpić-Oršić (2020) uses as main assumption the adoption of a Pierson–Moskowitz spectrum for each considered sea state combination H_s, T_p; therefore, the wind speed is derived by the formulations given in system (9). As the two equations of the system give different values for V_w except for the specific conditions identified by the wind–wave correlation, the method assumes that for each combination of H_s and T_p, the maximum wind speed between the two equations is used as reference V_w for the calculation. Such an approach allows an unique determination of V_w for each $H_s - T_p$ couple, estimating whether the DP system keeps position or not.

In this context, the scatter diagram approach produces two output types. The first is the quantitative evaluation of the DP operability in a sea area, obtained considering the wave occurrences and vessel headings:

$$OP_{DP} = \sum_{j=1}^{N_h} p_{h_j} \sum_{i=1}^{N_w} p_{w_i} I_{DP} \tag{10}$$

where p_h is the probability associated to each of the N_h vessel headings and p_w is the probability associated with the specific wave conditions given by the scatter diagram. The function I_{DP} is equal to 1 when the DP system holds the position, 0 otherwise.

Secondly, increasing the granularity of the calculations for H_s and T_p, the procedure is capable to identify critical curves for the DP system at the encounter angles χ of interest. The critical curve represents the operative limit for the DP system at each encounter angle, means the maximum sustainable $V_w - H_s$ for each T_p. Thus, DP critical curves clearly divide the $H_s - T_p$ diagram in two zones, one where I_{DP} is equal to 0 and the other where the function equals 1. Furthermore, the intersections between the critical curves and the P–M wind–wave correlation represent the couples $V_{W_{max}} - \chi$ of the conventional DP capability plot. Fig. 5 reports the correspondence between DP critical curves and the capability plot for the two reference vessels.

However, the main goal of the scatter diagram approach is the evaluation of DP operability in a given sea-area through the OP_{DP} index. To give an overview of the process, Table 5 reports the operability of the two reference vessels for Site A and Site B. The results refer to intact (all thrusters running) and single thruster failure conditions. As a general consideration, the scatter diagram approach highlights that the operability in Site B is higher than Site A for both vessels and all the investigated cases. Despite Site B presents higher H_s compared to Site A (Fig. 2), where the density of unfavourable $H_s - T_p$ conditions is higher for Site A. Such a conclusion cannot be achieved by analysing a standard deterministic capability plot only.

5. Enhanced modelling of long-term environmental conditions

Having detailed environmental data at disposal from local measurements or forecast models allows investigating alternative approaches for enhanced modelling of environmental conditions for site-specific DP predictions. Hindcast or forecast raw data include the principal parameters necessary for fitting long-term distributions, namely V_w, H_s and T_p.

Separate distributions can be derived for wind V_w and wave $H_s - T_p$ characteristics, giving the possibility to extend the capabilities of the

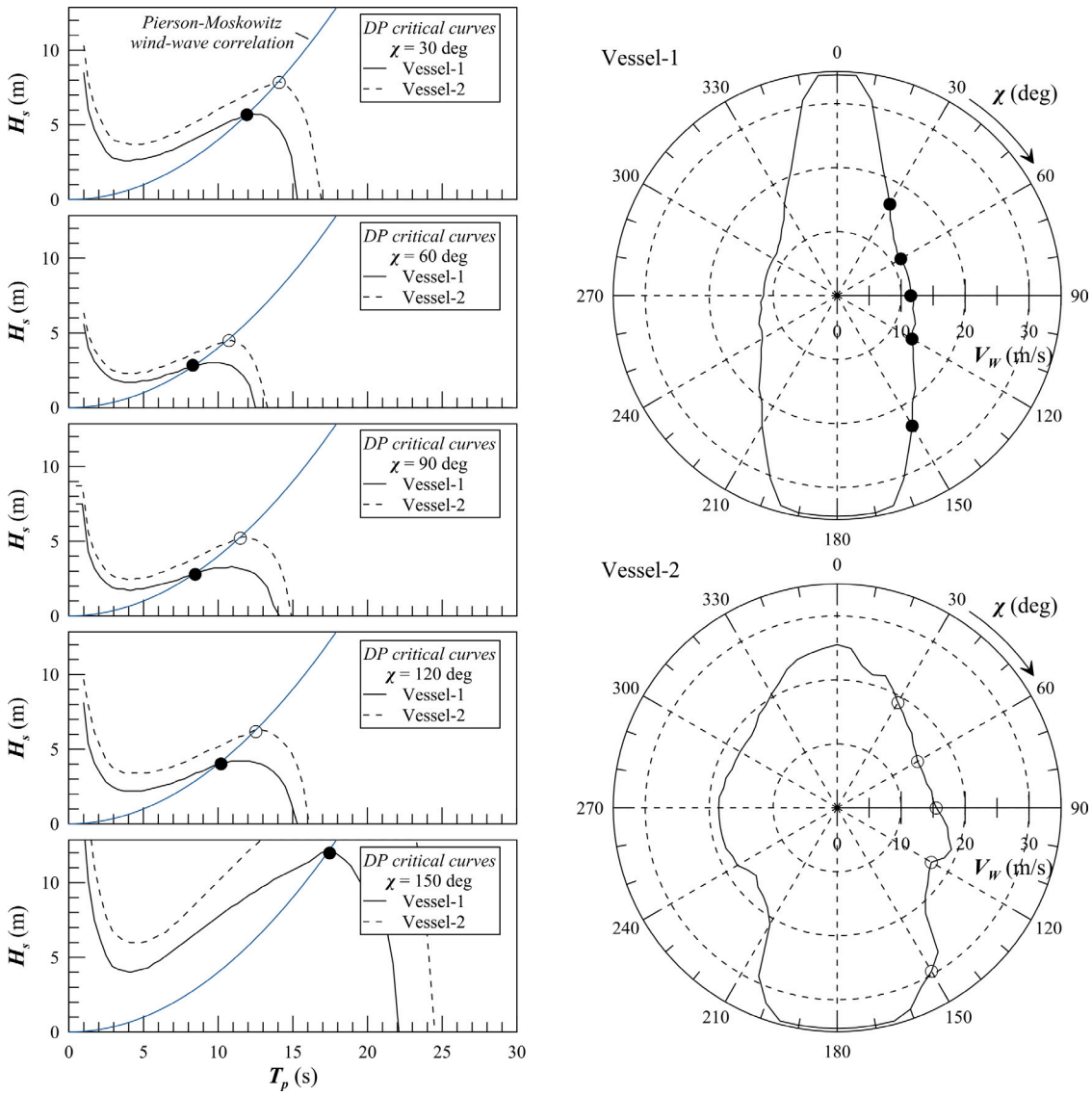

Fig. 5. Correspondence between site-specific DP critical curves and deterministic DP capability plots using the Pierson–Moskowitz wind–wave correlation for *Vessel-1* and *Vessel-2*.

Table 5
DP operability OP_{DP} for *Vessel-1* and *Vessel-2* according to scatter diagram approach.

Case	OP_{DP} (%)			
	Vessel-1		*Vessel-2*	
	Site A	Site B	Site A	Site B
Intact	74.26	75.46	91.36	92.05
T1-out	44.93	47.26	66.09	69.41
T2-out	46.43	48.82	72.38	74.88
T3-out	62.90	64.34	72.76	75.29
T4-out	62.90	64.34	78.96	81.40
T5-out	71.44	72.75	80.04	82.35
T6-out	–	–	75.05	77.87

scatter diagram approach, while keeping the same calculation assumptions. However a more useful option is to jointly combine wind and wave statistics to overcome the deterministic wind–wave correlation issue of the scatter diagram approach. Therefore, the possible usage of a trivariate wind–wave distribution is here described, underlining the need for a new dedicated calculation process to predict probabilistic DP operability.

5.1. Marginal V_w distribution

The starting point for the modelling of a joint long-term environmental condition is the identification of a marginal distribution for V_w. It has been widely observed that the probability density function f_{V_w} for the wind speed can be modelled with a two parameters Weibull distribution (DNV, 2014). In such a case, considering the random variable v_w in $(0, +\infty)$ for the wind velocity, the following relationship is valid:

$$f_{V_w}(v_w) = \frac{\beta_v}{\eta_v}\left(\frac{v_w}{\eta_v}\right)^{\beta_v - 1} e^{-\left(\frac{v_w}{\eta_v}\right)^{\beta_v}} \tag{11}$$

where β_v and η_v are the shape and scale parameter of the distribution, respectively. The distribution parameters vary with reference to the sea area, applying a proper fitting procedure to the measurements.

5.2. Bivariate joint $H_s - T_p$ distribution

Having at disposal only wave measurements data allows to establish a joint $H_s - T_p$ distribution f_{H_s,T_p}. Such a possibility provides an alternative to the scatter diagram approach, resulting in a continuous

joint distribution instead of a discrete one. The joint distribution for H_s and T_p is composed by a marginal distribution f_{H_s} and a conditional distribution $f_{T_p|H_s}$. Making reference to the two random variables h_s and t_p in $(0,+\infty)$ for wave height and period the following relationship is valid:

$$f_{H_s,T_p}(h_s,t_p) = f_{H_s}(h_s)\, f_{T_p|H_s}(t_p,h_s) \tag{12}$$

There are different probability distributions that can be used to fit f_{H_s}. An option is the adoption of a 2 parameter Weibull distribution (DNV, 2014) for V_w as in Eq. (11), or a hybrid fit between a Weibull and a log-normal distribution (Haver, 1980; Li et al., 2013). Concerning the joint distribution $f_{T_p|H_s}$, a log-normal model is widely agreed in the literature (Johannessen et al., 2001; Li et al., 2013; DNV, 2014):

$$f_{T_p|H_s}(t_p,h_s) = \frac{1}{\sqrt{2\pi}\sigma_{T_p} t_p} e^{-\frac{1}{2}\left(\frac{\ln t_p - \mu_{T_p}}{\sigma_{T_p}}\right)^2} \tag{13}$$

where standard deviation σ_{T_p} and mean value μ_{T_p} of $\ln t_p$ are expressed as smooth functions of h_s (Li et al., 2013). Adopting equation (13) as joint distribution together with a marginal distribution for H_s allows to have a continuous definition of the traditionally discrete scatter diagram.

However, it must be underlined that the above modelling of joint $H_s - T_p$ distribution remains still fully decoupled from the V_w statistics, leading to adopt same assumptions of the scatter diagram approach to determine the DP operability. A possible solution to couple the two loads, having detailed wind and wave data at disposal, is now described.

5.3. Trivariate joint $V_w - H_s - T_p$ distribution

Once both wind and wave statistics are available for the sites of interest it is possible to describe the long-term environmental statistics by means of a trivariate distribution, i.e. a joint $V_w - H_s - T_p$ distribution f_{V_w,H_s,T_p}. Such a distribution is composed by a marginal distribution f_{V_w} for the wind speed and two conditional distributions, $f_{H_s|V_w}$ for the wave height and $f_{T_p|V_w,H_s}$ for the periods. With this enhanced modelling, T_p is conditional to both H_s and V_w and not only to H_s as in Eq. (13). The resulting formulation for the trivariate distribution is:

$$\begin{aligned} f_{V_w,H_s,T_p}(v_w,h_s,t_p) = \; & f_{V_w}(v_w)\, f_{H_s|V_w}(h_s,v_w) \\ & f_{T_p|V_w,H_s}(t_p,h_s,v_w) \end{aligned} \tag{14}$$

where v_w, h_s and t_p are the random variables as previously defined. Once again, the marginal distribution for V_w is the one described by Eq. (11). For the conditional distribution $f_{H_s|V_w}$ an equivalent two parameters Weibull model can be used:

$$f_{H_s|V_w}(h_s,v_w) = \frac{\beta_h}{\eta_h}\left(\frac{h_s}{\eta_h}\right)^{\beta_h - 1} e^{-\left(\frac{h_s}{\eta_h}\right)^{\beta_h}} \tag{15}$$

Shape and scale parameter of the joint distribution are modelled as power functions of v_w, leading to the dependence of Eq. (15) to both v_w and h_s:

$$\begin{cases} \beta_h = & a_1 + a_2 {v_w}^{a_3} \\ \eta_h = & b_1 + b_2 {v_w}^{b_3} \end{cases} \tag{16}$$

where the regression parameters derive from non-linear fitting of raw data. For the conditional distribution $f_{T_p|H_s,V_w}$ the log-normal model of Eq. (13) can be used. However, the distribution parameters are now a function of h_s and v_w and not only of h_s. Therefore, to provide μ_{T_p} and σ_{T_p} the following regression models can be used:

$$\begin{cases} \mu_{T_p} = & \ln \dfrac{\mu^*_{T_p}}{\sqrt{\nu^2_{T_p}+1}} \\ \sigma_{T_p} = & \sqrt{\ln\left(\nu^2_{T_p}+1\right)} \\ \nu_{T_p} = & c_1 + c_2 e^{c_3 h_s} \\ \mu^*_{T_p} = & \overline{T_p}\left[1+\theta\left(\frac{v_w - \overline{v_w}}{\overline{v_w}}\right)^{\gamma}\right] \\ \overline{T_p} = & d_1 + d_2 h_s^{d_3} \\ \overline{v_w} = & e_1 + e_2 h_s^{e_3} \end{cases} \tag{17}$$

The regression parameters for the trivariate joint distribution described by Eqs. (15) (16) (17) are reported in Table 6 for *Site A* and *Site B* according to the analysis performed by Li et al. (2013).

5.4. Implications for operability calculations

The adoption of joint-distributions for the environmental modelling influences the way operability should be assessed through equation (10). Considering the case of the bivariate $H_s - T_p$ distribution (equation (12)), the determination of the DP system operability can be derived as a direct integration of Eq. (10), by using a Monte Carlo process (as described in the following sections) for each angle χ. In such a way, the OP_{DP} index is no more subject to the discretisation given by the scatter diagram.

For the trivariate joint distribution of Eq. (14), there is no more an unique correspondence between H_s, T_p and V_w, which is required to apply the scatter diagram approach. Therefore, the evaluation of the operability according to Eq. (10) has to be modified, as already highlighted for the case of the joint $H_s - T_p$ distribution.

The following section presents the newly proposed DP operability calculation based on an MC process using joint-distributions for the environmental conditions.

6. DP operability calculation as a Monte Carlo process

Adopting the enhanced environmental modelling described in Section 5, the determination of the DP operability may follow a non-deterministic multidimensional Monte Carlo (MC) integration process. The general approximation of a MC integral has the following form:

$$\int_{\Omega} f(\mathbf{x})\,\mathrm{d}\mathbf{x} \approx \frac{1}{N_s}\int_{\Omega}\mathrm{d}\mathbf{x}\sum_{i=1}^{N_s} f(\mathbf{x}_i) \tag{18}$$

where $\Omega \subset \mathbb{R}^m$ is an m-dimensional probability space, $\mathbf{x} \in \Omega$ is a set of m independent random variables and N_s is the number of samples. It is convenient to define Ω as an unit hypercube $(0,1)^m$ leading to $\int_{\Omega}\mathrm{d}\mathbf{x} = 1$, and to use uniform random variables $\mathbf{U} \sim \mathbb{U}(0,1)$ to define $\mathbf{x}$. Then, Eq. (18) assumes the following form:

$$\int_{\Omega} f(\mathbf{x})\,\mathrm{d}\mathbf{x} \approx \frac{1}{N_s}\sum_{i=1}^{N_s} f(\mathbf{U}_i) \tag{19}$$

Eq. (10), defining OP_{DP} in the scatter diagram approach, can be converted in the form of a sum of MC integrals, using the joint $H_s - T_p$ distribution previously described for the N_h heading angles of interest. Then the OP_{DP} formulation becomes:

$$OP_{DP} = \sum_{j=1}^{N_h} p_{h_j}\frac{1}{N_s}\sum_{i=1}^{N_s} f_{H_s,T_p}(\mathbf{U})\, I_{DP_i} \tag{20}$$

The same process may suit also for the trivariate joint $V_w - H_s - T_p$ distribution described in Eqs. (14) to (18). Therefore, the corresponding MC-like formulation for the operability index assumes the following form:

$$OP_{DP} = \sum_{j=1}^{N_h} p_{h_j}\frac{1}{N_s}\sum_{i=1}^{N_s} f_{V_w,H_s,T_p}(\mathbf{U})\, I_{DP_i} \tag{21}$$

Table 6
Parameters of the joint $V_w - H_s - T_p$ distribution for Site A and Site B.

	f_{V_w}		$f_{H_s\|V_w}$						$f_{T_p\|V_w,H_s}$										
Site	η_v	β_v	a_1	a_2	a_3	b_1	b_2	b_3	c_1	c_2	c_3	d_1	d_2	d_3	e_1	e_2	e_3	θ	γ
Site A	2.002	7.866	1.643	0.093	1.000	1.969	0.031	1.644	5.000	5.970	0.223	1.000	4.055	0.466	0.030	0.234	−0.221	−0.143	1.000
Site B	2.029	9.409	2.136	0.013	1.709	1.816	0.024	1.787	8.000	1.938	0.486	2.500	3.001	0.745	−0.001	0.316	−0.145	−0.255	1.000

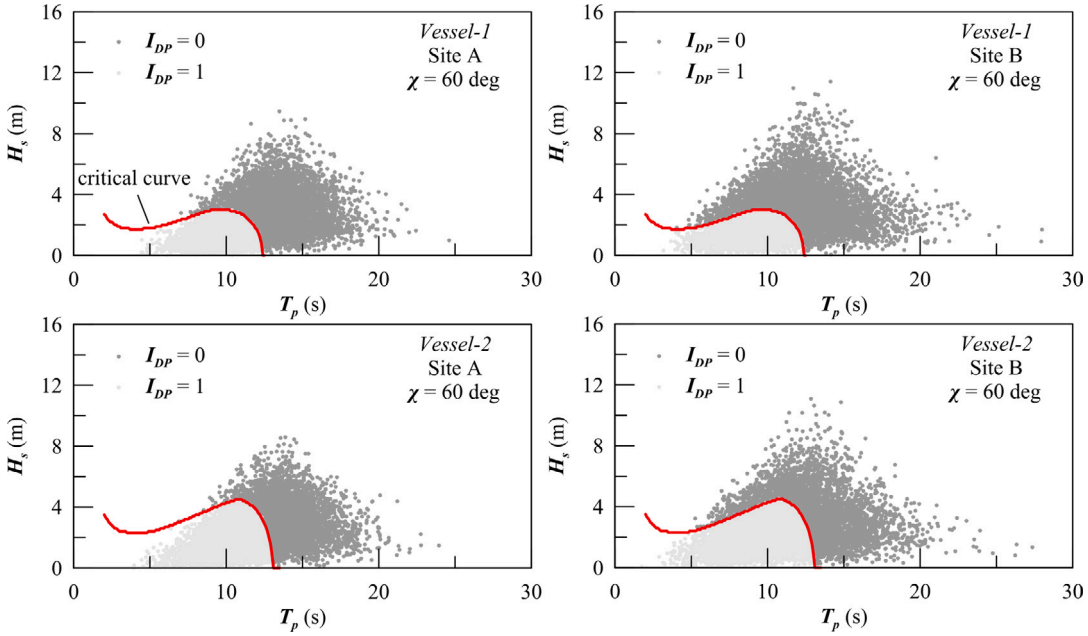

Fig. 6. Example of crude Monte Carlo process for DP operability (χ=60 deg), sampling H_s and T_p from a bivariate joint distribution.

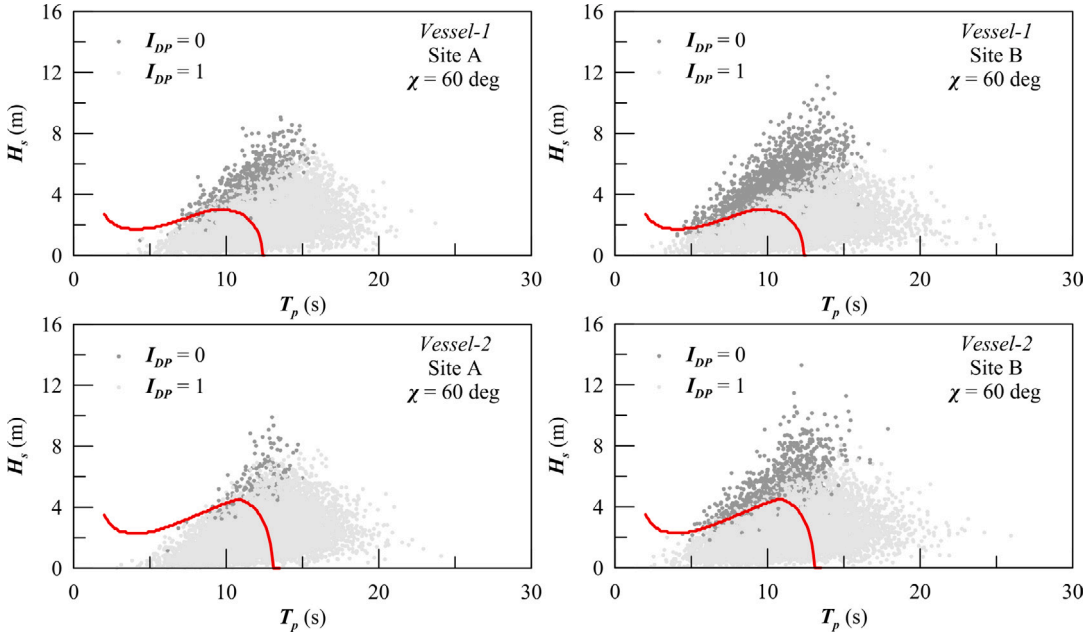

Fig. 7. Example of crude Monte Carlo process for DP operability (χ=60 deg), sampling H_s, T_p and V_w from a trivariate joint distribution.

From the above Eqs. (20) and (21), it is evident that the environmental joint distributions are direct functions of the uniform random variables **U**. Therefore, the sampling method adopted to generate the random distributions influences the final integration. The common practice for MC integration is performing a direct sampling of **U** with pseudo-random numbers, adopting the so-called *crude MC method* (Hammersley and Handscomb, 1964). As the final joint distributions are non-uniform, the associated random variables should be

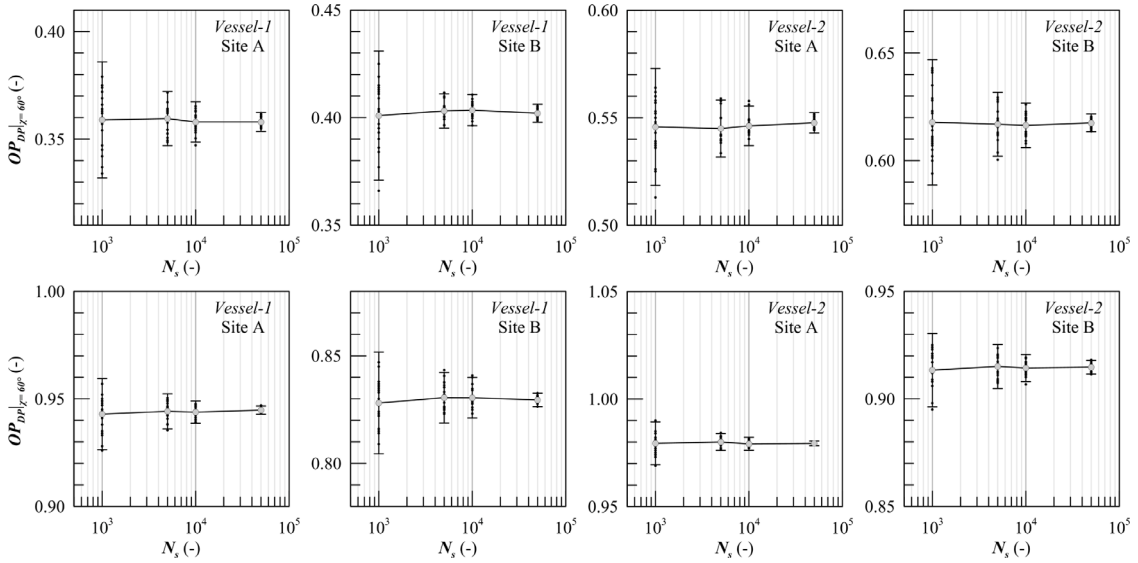

Fig. 8. μ and 2σ interval for DP operability at χ=60 deg using a bivariate (*top*) and trivariate (*bottom*) joint-distribution for the environmental conditions.

Table 7
DP operability at χ=60 deg using crude MC method with 20 repetitions and increasing sample sizes.

		$OP_{DP}\|_{\chi=60°}$ (%)							
		Joint $H_s - T_p$				Joint $V_w - H_s - T_p$			
		Vessel-1		*Vessel-2*		*Vessel-1*		*Vessel-2*	
		Site A	Site B	Site A	Site B	Site A	Site B	Site A	Site B
$N_s = 1 \cdot 10^3$	μ	35.89	40.10	54.58	61.78	94.29	82.81	97.94	91.34
	$CI(95\%)$	±1.35E0	±1.50E0	±1.36E0	±1.46E0	±8.26E−1	±1.18E0	±4.97E−1	±8.54E−1
$N_s = 5 \cdot 10^3$	μ	35.95	40.31	54.50	61.69	94.42	83.05	98.00	91.51
	$CI(95\%)$	±6.29E−1	±3.98E−1	±6.63E−1	±7.43E−1	±4.08E−1	±5.89E−1	±1.98E−1	±5.10E−1
$N_s = 1 \cdot 10^4$	μ	35.80	40.34	54.62	61.64	94.38	83.05	97.91	91.43
	$CI(95\%)$	±4.69E−1	±3.59E−1	±4.60E−1	±5.17E−1	±2.59E−1	±4.72E−1	±1.52E−1	±3.16E−1
$N_s = 5 \cdot 10^4$	μ	35.80	40.20	54.76	61.75	94.48	82.95	97.94	91.47
	$CI(95\%)$	±2.20E−1	±2.10E−1	±2.38E−1	±2.07E−1	±9.50E−2	±1.57E−2	±5.51E−2	±1.60E−1

derived from the sampled **U**. The most commonly adopted method is given by the inversion of the cumulative density function $F(x)$. Therefore, being **U** uniform in $[0,1]$, $F^{-1}(\mathbf{U})$ is distributed according to F, and, for a generic variable X, the cumulative $F(\mathbf{X})$ is consequently uniform in $[0,1]$. This property is valid also for multidimensional variables and applies to the joint-distributions described above.

Fig. 6 shows for the reference angle χ of 60 degrees an example of the application of a crude MC process for OP_{DP} calculation of the two reference vessels in Site A and Site B. The example refers to the bivariate case (12) and described by Eq. (20) for N_h=1 and p_{h_1}=1, considering $N_s = 10^4$ samples. The plot shows that the cases with $I_{DP} = 1$ and the cases where $I_{DP} = 0$ lay in two distinct regions of the $H_s - T_p$ space. These two zones are divided by the DP critical curve (displayed in red) obtained with the scatter diagram approach, as described in Section 4.2. The wind–wave correlation derives from the same assumptions used to calculate V_w from the distinct couples $H_s - T_p$.

Fig. 7 represents the same scenarios of Fig. 6 but sampling the environmental conditions from the trivariate $V_w - H_s - T_p$ joint distribution given in Eq. (14) and OP_{DP} given by (21). For such conditions it is not possible to clearly distinguish two regions on the $H_s - T_p$ space having $I_{DP} = 1$ and $I_{DP} = 0$. Consequently, there is no correlation between the DP critical curve given by the scatter diagram approach and the MC process with a trivariate distribution. The main reason for this effect is the presence of the marginal distribution for V_w instead of the simplified deterministic modelling of the scatter diagram approach. It is also clearly visible that the wind distribution affects the final value of the OP_{DP}.

The cases reported in Figs. 6 and 7 refer to a single run performed with a crude MC integration with 10^4 samples. Since the random nature of the sampling process leads to different couples or triplets of environmental parameters at each run, the final integral value and the convergence history are different at each calculation. As the approximated integral converges to an exact value as N_s increases without upper bounds, then the process is subject to uncertainties. Therefore, the use of a crude MC method requires to adopt a sufficiently large number of samples that ensures the matching of a required confidence level for the solution. This can be achieved by calculating a Confidence Interval (CI) across multiple repetitions N_r with different sample size N_s.

Considering the same conditions of the examples reported in Figs. 6 and 7 a set of $N_r = 20$ repetitions with different sample size N_s ranging from 10^3 to $5 \cdot 10^4$ has been performed. Being N_r not large enough to ensure that CI can be described by a normal distribution, the following formulation has been adopted:

$$CI(c) = \mu \pm t \frac{\sigma}{\sqrt{N_r}} \tag{22}$$

where μ is the mean value of the N_r repetitions, σ is the repetitions variance and t is the inverse cumulative density function of the Student t-distribution with confidence level c and $N_r - 1$ degrees of freedom. Fig. 8 shows μ with the associated 2σ interval obtained for the reference vessels and conditions using the bivariate and the trivariate joint distributions. Table 7 reports μ and the 95% CI for the considered cases and the operability in percentage.

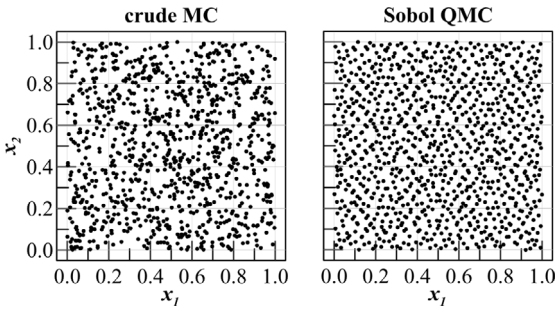

Fig. 9. Bi-dimensional uniform distribution according to crude MC and Sobol QMC ($N_s = 10^3$).

The results show that the mean value for the operability is only slightly affected by N_s, as the differences are in the range of 0.25% OP_{DP} for both bivariate and trivariate joint-distribution cases. On the contrary, N_s strongly influences the CI, highlighting the necessity to perform a large amount of simulation to reach stability on multiple repetitions. Fig. 8 clearly shows the spread in the results obtained by multiple repetitions with same N_s, and how the spread reduces when increasing the sample size. Furthermore, it is also clear that σ, and consequently CI, reduces as μ is closer to unit. Also considering the cases where the CI is lower, uncertainties always affect the first or second decimal digit of the μ value, while considering OP_{DP} as a percentage. Therefore, with the adoption of a crude MC process, the final value of OP_{DP} depends on the convergence and variance of the integration process, thus on the selection of both N_s and N_r.

Even if the obtained OP_{DP} values for the bivariate case differ from the trivariate case, they are comparable with the scatter diagram approach. This can be expected for the wave distributions in Fig. 2 and is confirmed by the partial OP_{DP} values derived from scatter diagram calculations (using the granularity of Fig. 2). For Site A the values OP_{DP} for $\chi = 60$ deg are 35.70% and 54.90% for *Vessel-1* and *Vessel-2*, respectively; for Site B: 40.51% and 61.71%. Therefore, crude MC with a joint $H_s - T_p$ gives no additional information compared to the quasi-probabilistic scatter diagram approach.

Therefore, for practical applications, it is convenient to implement a process that is still capable to sample joint-distribution while reducing the variability of a crude MC integration.

6.1. Quasi-Monte Carlo sampling for the joint $V_w - H_s - T_p$ distribution

An alternative sampling strategy, aimed to reduce the variance of MC integration, is the adoption of Quasi-random methods (Niederreiter, 1987), distributing samples in Ω as uniformly as possible with a deterministic approach. Thanks to the adoption of low-discrepancy sequences it is possible to achieve lower errors than crude MC on practical integration problems (Niederreiter, 1992). Between the different deterministic low-discrepancy sequences, the Sobol chain presents an attractive option, giving a good reproduction of the uniform distribution even with a low sample size and without high computational effort (Sobol et al., 2011). Furthermore, the process needed to generate Sobol sequences can be easily implemented in software programs (Levitan et al., 1988; Bradley and Fox, 1988). When a Quasi-random method is used to sample uniform or generic distributions, it is common to adopt the nomenclature of Quasi-Monte Carlo (QMC) sampling.

Fig. 9 shows the differences between crude MC and QMC with Sobol sequences for the sampling of a bivariate uniform distribution with 10^3 samples. This example highlights the differences in the coverage of a sampling space given by the two procedures. QMC method grants a more uniform coverage with a lower number of samples, avoiding agglomeration of points and void spaces typical of a crude MC approach.

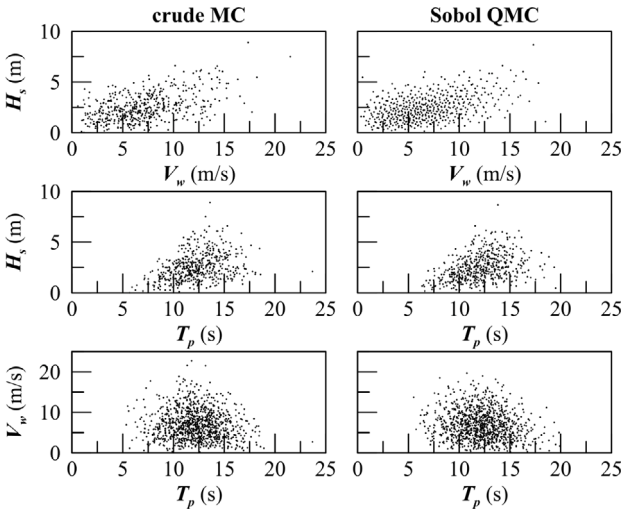

Fig. 10. Joint $V_w - H_s - T_p$ distribution for Site-A according to crude MC and Sobol QMC ($N_s = 10^3$).

The adoption of a QMC sampling to non-uniform distributions follows the same concept of the MC sampling and can be addressed with the inversion of the cumulative distribution. In the specific case of the joint $V_w - H_s - T_p$ distribution, the QMC sampling process to obtain V_w, H_s and T_p can be summarised in the following steps:

1. Generation of $\mathbf{U} = \left(u_{V_w}, u_{H_s}, u_{T_p}\right) \in [0,1]^3$ with a Sobol sequence.
2. Compute $F^{-1}_{V_w}\left(v_w\right)$ from the probability density function (PDF) given in Eq. (11).
3. Compute $F^{-1}_{H_s|V_w}\left(h_s, v_w\right)$ from the PDF given in Eq. (15).
4. Compute $F^{-1}_{T_p|H_s,V_w}\left(t_p, h_s, v_w\right)$ from the PDF given in Eq. (13).
5. Compute V_w, H_s and T_p as follows:

$$\begin{cases} V_w = & F^{-1}_{V_w}\left(u_{V_w}\right) \\ H_s = & F^{-1}_{H_s|V_w}\left(u_{H_s}|_{V_w}\right) \\ T_p = & F^{-1}_{T_p|H_s,V_w}\left(u_{T_p}|_{H_s,V_w}\right) \end{cases} \tag{23}$$

Applying the above steps, it is possible to generate N_s samples of the joint environmental characteristics for a specific area. Fig. 10 compares the sampling of 10^3 triplets $V_w - H_s - T_p$ for Site A (using the parameters in Table 6 for the joint distribution) resulting from crude MC and QMC processes. From the reported example it is evident that the QMC process improves the coverage of the sample space also for joint-distributions, avoiding agglomeration of samples and unfilled spaces, as already stated for the uniform distributions.

Adopting a deterministic Sobol sequence of numbers, the process is no more stochastic, thus it allows to determine an unique value across multiple repetitions. Fig. 11 shows, for the same cases reported in Fig. 7, the convergence history of the QMC integration process compared to 5 of the 20 repetitions of MC runs performed with $5 \cdot 10^4$ samples each. The graphs show also μ and the interval 2σ of the MC runs with different N_s values. It can be observed that the results of QMC integration start to oscillate around the final value when N_s is above 10^3 for cases where the partial OP_{DP} is above 0.90 for *Vessel-2* in Site A, and above $5 \cdot 10^3$ for the other cases. Moreover, the value of the single QMC run is close to the mean of the 20 MC repetitions, except for $N_s = 10^3$, where σ value for MC integrations is significant, leading to high spread of the solutions.

Even though the QMC method does not require multiple repetitions of the same run, it is still necessary to identify the number of samples

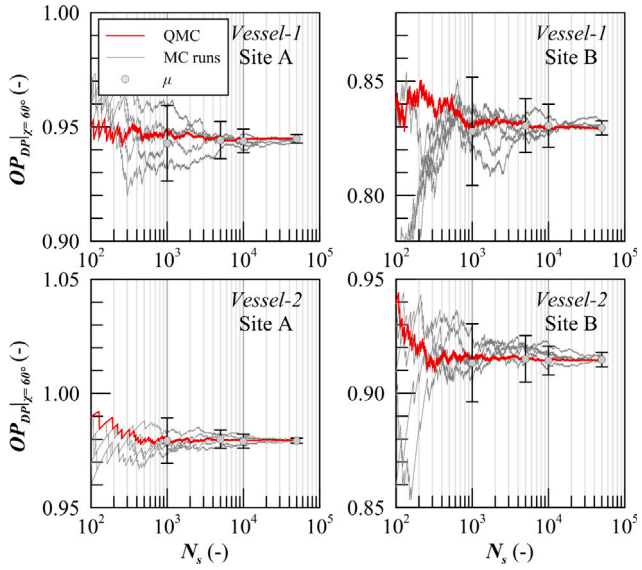

Fig. 11. Solution history for the partial OP_{DP} at $\chi = 60$ deg with MC and QMC process.

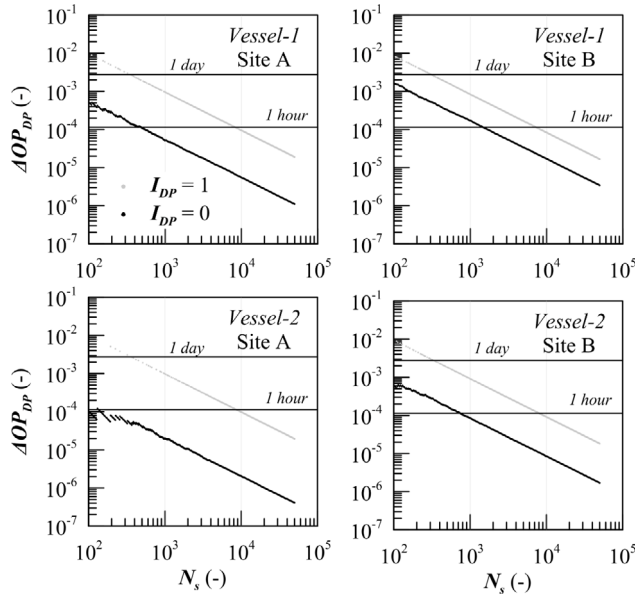

Fig. 12. QMC integration convergence for the partial OP_{DP} at $\chi = 60$ deg.

N_s that ensures a sufficient level of convergence to the partial OP_{DP} value at a given angle χ of the environmental loads. The convergence can be evaluated checking the relative differences between partial OP_{DP} at consecutive samples:

$$\Delta OP_{DP_k} = \left| \sum_{i=1}^{k} \frac{I_{DP_i}}{k} - \sum_{i=1}^{k-1} \frac{I_{DP_i}}{k-1} \right| \quad \text{for } k = 2, \dots, N_s \tag{24}$$

Attention should be given to the convergence threshold to be considered for the integral. Being the partial OP_{DP} a quantity defined between 0 and 1 that indicates the fraction of year a vessel could operate in a sea area at a given encounter angle, the convergence should be related to the time unit used to quantify the operability. In case it is quantified in days, considering 1 day as convergence threshold, the convergence can be reached when ΔOP_{DP} approaches $2.74 \cdot 10^{-3}$. Considering a threshold of 1 h, then the ΔOP_{DP} of reference is $1.14 \cdot 10^{-4}$.

Fig. 12 shows the ΔOP_{DP} variations with N_s for the same test cases previously used in this section. For each case it is possible to distinguish

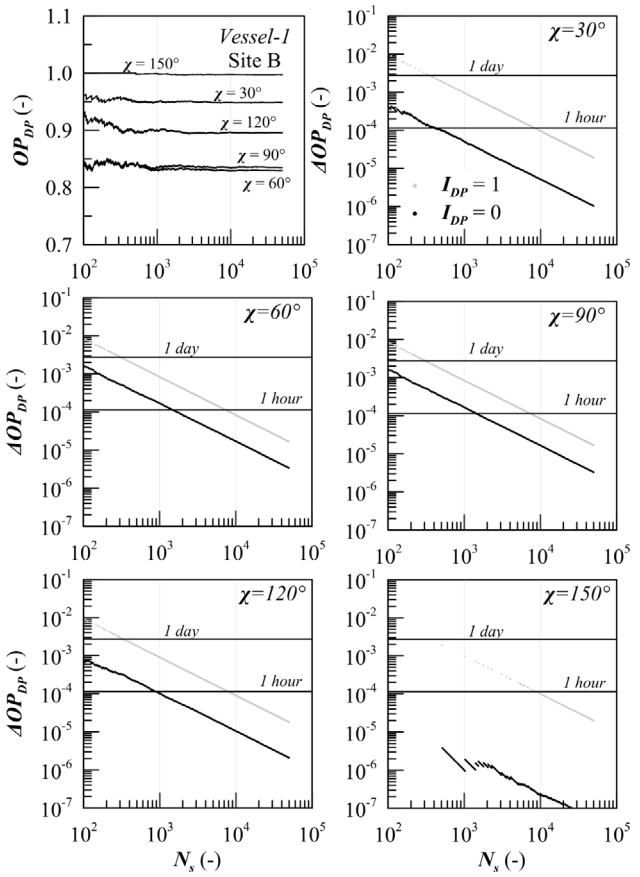

Fig. 13. QMC integration convergence for the partial OP_{DP} at multiple χ for *Vessel-1* in Site-B.

two curves (approximate to straight lines in the logarithmic scale of the figure): one for the cases with $I_{DP} = 1$ and the other with $I_{DP} = 0$. Having the integrating function I_{DP} only two possible discrete values, the convergence curve is not continuous. For such a reason, the level of convergence for the ΔOP_{DP} should be checked on the sequence of points referring to $I_{DP} = 1$, the higher of the two sequences shown in the graphs. Fig. 12 reports also the two thresholds representing the accuracy of 1 day and 1 h convergence values. It can be observed that, for all the tested cases, the convergence at 1 day level is reached after 300–400 samples, the 1 h level at about 10^4 samples. When the partial OP_{DP} is high, then the convergence is reached for a higher number of samples. This is due to the higher occurrence of cases with $I_{DP} = 1$ compared to conditions where partial OP_{DP} value is below 0.9.

The reported cases refer to $\chi = 60$ deg. To check the behaviour of the convergence with N_s at different headings, an additional set of simulations has been performed, reporting here the case for $Vessel - 1$ in Site B. Fig. 13 shows the convergence of the partial OP_{DP} for the headings of 30, 60, 90, 120 and 150 degrees. The behaviour of the ΔOP_{DP} at the different encounter angles reflects the considerations given for the analyses provided for $\chi = 60$ degrees. Therefore, it can be concluded that a $N_s = 10^4$ can be sufficient to reach a level of convergence around 1 h for the partial OP_{DP} index.

6.2. DP operability evaluation

The QMC process described in the previous section is oriented to obtain the partial OP_{DP} indices specific for a heading angle χ. According to Eq. (21) the partial indices should be summed and weighted for the p_h associated to each specific χ. In case the operative profile of the offshore vessel requires to operate at preferential χ angles, p_h factors

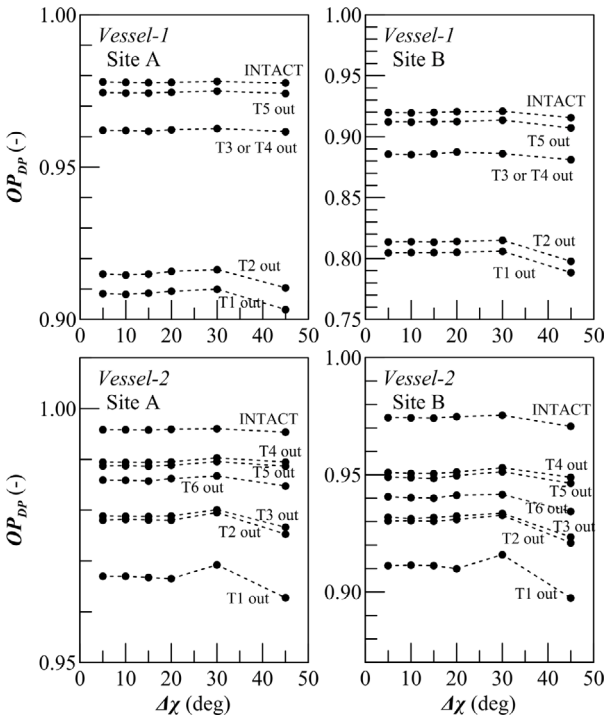

Fig. 14. OP_{DP} dependence from $\Delta\chi$ values.

may be not homogeneous and should be specified by the operator. However, for a global and general assessment of the DP operability in a given sea area, the p_h can be assumed homogeneous, thus considering that χ angles have the same occurrence $1/N_h$. Therefore, Eq. (21) can be rewritten in the following form:

$$OP_{DP} = \frac{1}{N_h}\sum_{j=1}^{N_h} OP_{DP}|_{\chi_j} \tag{25}$$

where $OP_{DP}|_{\chi}$ is the partial OP_{DP} at a given angle χ. The direct application of Eq. (25) for OP_{DP} predictions is not advisable and should be done with caution, as the usage of a not sufficiently high discrete number of headings may lead to inaccuracy in the final results. In case the partial OP_{DP} are not of specific interest for the end user, the QMC process can also include the heading by sampling χ as an additional independent random variable with uniform distribution in $[0, 2\pi]$.

As it is convenient to identify the headings with lower partial operability, it is advisable to maintain the calculation process within a discrete number of χ angles, adopting then an approximate integration procedure for the final OP_{DP}. To this end, the adoption of a Simpson integration method could help keeping a discrete number N_h of χ angles. In such a case, Eq. (25) becomes:

$$\begin{aligned} OP_{DP} &= \tfrac{1}{2\pi}\int_0^{2\pi} f(\chi)\,\mathrm{d}\chi \\ &\approx \tfrac{\Delta\chi}{6\pi}\left[f(0) + 2\sum_{j=1}^{N_h/2-1} f\left(\chi_{2j}\right)\right. \\ &\left. +4\sum_{j=1}^{N_h/2} f\left(\chi_{2j-1}\right) + f(2\pi)\right] \end{aligned} \tag{26}$$

where $f(\chi)$ is the abbreviation for $OP_{DP}|_{\chi}$. Eq. (26) is valid for χ in radiant, but substituting 2π with 360 it becomes valid also for χ in degrees.

Fig. 14 shows the dependence of the final OP_{DP} from the $\Delta\chi$ value, applying equation (26) to the two reference vessels in Site A and Site B with no thruster failures (intact condition) and all possible single thruster failures. Using six different $\Delta\chi$, ranging from 5 to 45 degrees, the variations are negligible between $\Delta\chi$=5, 10 and 15 degrees. Increasing the step, variation in the final OP_{DP} raises up to the previously mentioned accuracy threshold of 1 day for 1 year of operation. This is true especially for failure conditions, where the value of OP_{DP} is lower than for intact case. In general, the lower is the OP_{DP} the higher is the importance to choose a low $\Delta\chi$.

Table 8
DP operability OP_{DP} for *Vessel-1* and *Vessel-2* according to QMC process.

Case	OP_{DP} (%)			
	Vessel-1		*Vessel-2*	
	Site A	Site B	Site A	Site B
Intact	97.79	91.98	99.58	97.44
T1-out	90.85	80.47	96.70	91.12
T2-out	91.49	81.36	97.80	93.03
T3-out	96.20	88.58	97.89	93.19
T4-out	96.20	88.58	98.87	94.90
T5-out	97.45	91.21	98.95	95.10
T6-out	–	–	98.59	94.06

Table 8 reports the OP_{DP} values, in percentage form, for the reference cases obtained with the lower of the tested steps $\Delta\chi$ of 5 degrees, being the one granting the better visualisation of the partial OP_{DP} results in polar form, as depicted in Fig. 15. Data in tabular form refer to the intact condition and all the possible single thruster failures. The graphical plot shows the intact condition and the minimum envelope of the single thruster failures, means the minimum partial OP_{DP} at each angle between the single failure options.

Observing the values provided in Table 8, it is possible to quantify the differences between operability in the two sea sites for the reference vessel. Site A is the most favourable area for both the analysed offshore units, leading to about 8 unworkable days in one year for *Vessel-1* and 1.5 days for *Vessel-2*, both with all thrusters running. The unworkable days in Site B raise to about 29 days for *Vessel-1* and 9.5 for *Vessel-2*. Concerning the single failure cases, the most restrictive failure for both vessels is the loss of the foremost actuator T1. For such a failure, *Vessel-1* cannot operate for about 33 days in Site A and 71 days in Site B; *Vessel-2* cannot operate for 12 days in Site A and 32.5 days in Site B.

The polar plots in Fig. 15 highlight the differences not only in the global operability, but also in the partial indices. It is possible to identify the χ angles that are most critical for the vessel operation, both in intact condition and with thruster failures. For *Vessel-1*, being the DP system symmetric with respect to vessels' diametral plane, the DP_{OP} plots are also symmetric between starboard and port side headings. This is true also for the single failure envelope, as also failures are intrinsically symmetric. For this vessel, the most critical headings are around 60 and the symmetric 300 degrees. *Vessel-2* presents an asymmetric DP system layout with additional asymmetry induced by the external pipe load. This reflects on the resulting operability plots, where 60 degrees is also here the most critical heading for operability. However, for port headings the worst case is around 240 degrees both for intact and failure minimum envelope conditions.

Comparing the results of Table 8 with the ones from the scatter diagram approach in Table 5, a difference between 20 and 40% can be observed in the final operability index OP_{DP} for all the tested cases, which is essentially due to the different assessment of wind speed V_w. This underlines even more the importance of a proper modelling of environmental conditions for DP predictions.

Concerning the computational time, the evaluation of partial OP_{DP} for a single heading χ with $N_s = 10^4$ takes in mean 1 min on a regular laptop without parallelisation. Therefore, the cases reported in this example with 73 headings take about 1 h and 12 min each, but time can be significantly reduced varying the $\Delta\chi$ and running calculation in parallel. The calculation time is higher than in the scatter diagram approach, as QMC process evaluates more environmental conditions, but the global calculation time makes this approach still applicable for design and analysis purposes.

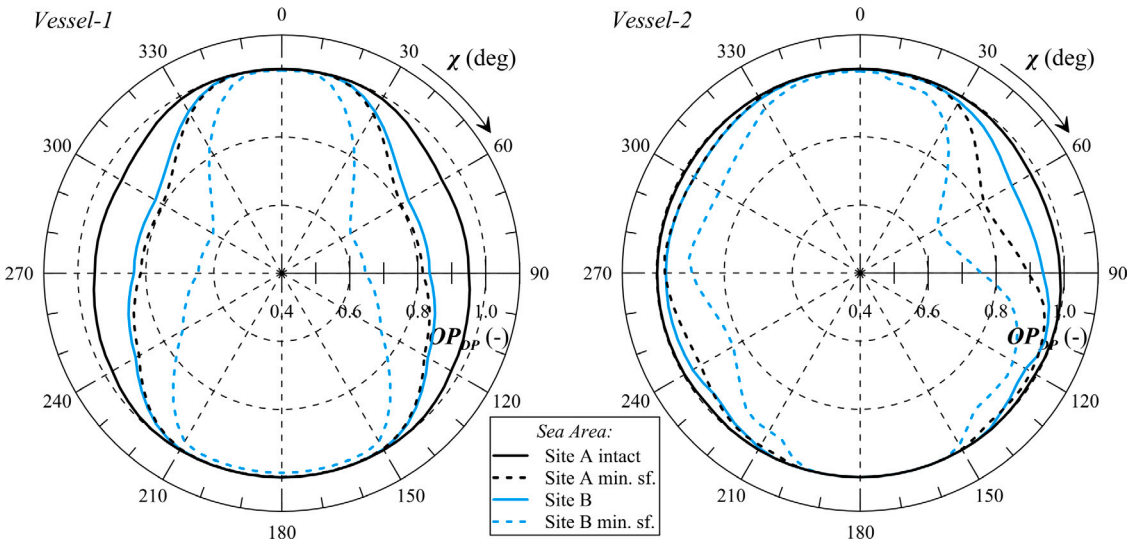

Fig. 15. Partial OP_{DP} polar plots for the reference vessels in Site A and Site B considering all thrusters running (*intact*) and minimum envelope of single failures (*min. sf.*).

7. Recovering the capability plot

The developed site-specific probabilistic operability prediction method based on the sampling of a multivariate distribution presents the DP capability in terms of operability in a given area. This is the same vision of the scatter diagram approach. However, offshore operators are more familiar with conventional capability plots for DP system evaluation, thus by associating DP performance limits with a maximum sustainable wind speed varying with χ.

The scatter diagram approach, as highlighted in Mauro and Prpić-Oršić (2020), is not capable to reproduce an equivalent capability plot representing the wind limit, being the wind directly evaluated by H_s and T_p according to Eqs. (9). The most similar output to a capability plot provided by the scatter diagram approach is the determination of the V_w associated to the minimum H_s at which the DP system cannot keep position at the different χ angles (see Fig. 5).

With the adoption of the joint $V_w - H_s - T_p$ distribution for the environmental parameters, there is no more a single V_w for each couple $H_s - T_p$, since V_w follows the marginal distribution given by Eq. (11). Analysing the results of the QMC process for the partial OP_{DP} at different χ angles it is possible to distinguish between favourable ($I_{DP} = 1$) and unfavourable ($I_{DP} = 0$) cases as a function of V_w. This kind of analysis generates two sub-distributions, with associated probability density p as a function of V_w, one for $I_{DP} = 1$ and another for $I_{DP} = 0$. Besides establishing the probability of the two possible values of I_{DP}, it is convenient to determine the relative frequency f^* of favourable and unfavourable cases for specific intervals ΔV_w:

$$\begin{cases} f_0^*\left(\Delta V_w\right)_i &= \frac{n_{0i}}{N_{V_i}} \\ f_1^*\left(\Delta V_w\right)_i &= \frac{n_{1i}}{N_{V_i}} = 1 - f_0^*\left(\Delta V_w\right)_i \end{cases} \tag{27}$$

where n_0 is the number of cases with $I_{DP} = 0$ inside the ith interval ΔV_w, n_1 is the number of cases with $I_{DP} = 1$ and N_V is the total number of samples in the ith interval ΔV_w.

The adoption of relative frequency is different from considering an empirical probability density function. The relative frequency f^* directly indicates the ratio between favourable and unfavourable cases in specific V_w intervals. Therefore, it is possible to identify which are the V_w intervals that are leading to more unfavourable than favourable cases. Being the wind loads function of V_w^2 (as shown in Eq. (6)), it is reasonable suppose that increasing V_w, $f_0^*\left(\Delta V_w\right)$ increases too, and also the associated H_s will be higher in average (according to the conditional distribution of Eq. (15)) as well as T_p. This implies that, using a sufficient number of samples, $f_0^*\left(\Delta V_w\right)$ monotonically increases with V_w. Then, evaluating f^* for all the consecutive ΔV_w, it is possible to identify the V_w leading to a desired value of f^* with a simple interpolation.

Repeating the process for all the χ angles it is possible to extract all the V_w that correspond to a selected relative frequency value. As an example, selecting a $f^* = 0.5$ the limiting wind speed where it becomes less frequent the ability to keep the desired position at the considered χ angle can be identify. Reporting the wind speed in a polar plot consequently leads to the determination of a capability plot specific for the considered sea area.

To clarify the procedure, Fig. 16 shows the determination of the two sub-populations of favourable and unfavourable cases and the associated frequencies f^* for both the two reference vessels in Site B. The graphic example shows the χ angles of 30, 60, 90 and 120 degrees for the intact condition. It can be observed that, being the partial DP_{OP} relatively high for all the headings (see Fig. 15), the population with $I_{DP} = 1$ is predominant and follows the behaviour of the Weibull marginal distribution defining V_w. The population with $I_{DP} = 0$ covers the higher wind speeds and has a density function more similar to a Normal distribution. In the same figure it is possible to observe the relative frequency f^* that confirms the monotonic behaviour. Comparing the results for the two vessels it is possible to identify that, being OP_{DP} higher for *Vessel-2*, the population of unfavourable cases presents a narrower peak for *Vessel-2* and, therefore, corresponds to an identification of higher V_w associated to f^*=0.5.

Fig. 17 shows the obtained probabilistic-based capability plots for the two vessels in both Site A and Site B, comparing them with the conventional capability plot obtained with IMCA wind–wave correlation and the site-specific wind–wave correlations. The Figure shows the curve referring to f^*=0.5 together with the band $0<f^*<1$, thus the whole range of V_w where DP system may not counteract the external loads. As a general remark, it should be underlined that in case the partial OP_{DP} is equal to 1 for a given χ, the associated limiting V_w derived for the site-specific capability plot is equal to the maximum V_w sampled from the marginal wind distribution. Therefore, for headings close to 0 and 180 degrees the site-specific capability curves are saturated to the relative maximum wind speeds of Site A and Site B. This behaviour is in line with the capability plots obtained with site-specific wind–wave correlations, which are also defined up to a maximum wind speed.

Considering the curve for f^*=0.5, the reported example shows an agreement with the shapes of the limiting curve obtained with conventional method. For *Vessel-1*, the behaviour of the probabilistic site-specific capability curves is more coherent with the Pierson–Moskowitz

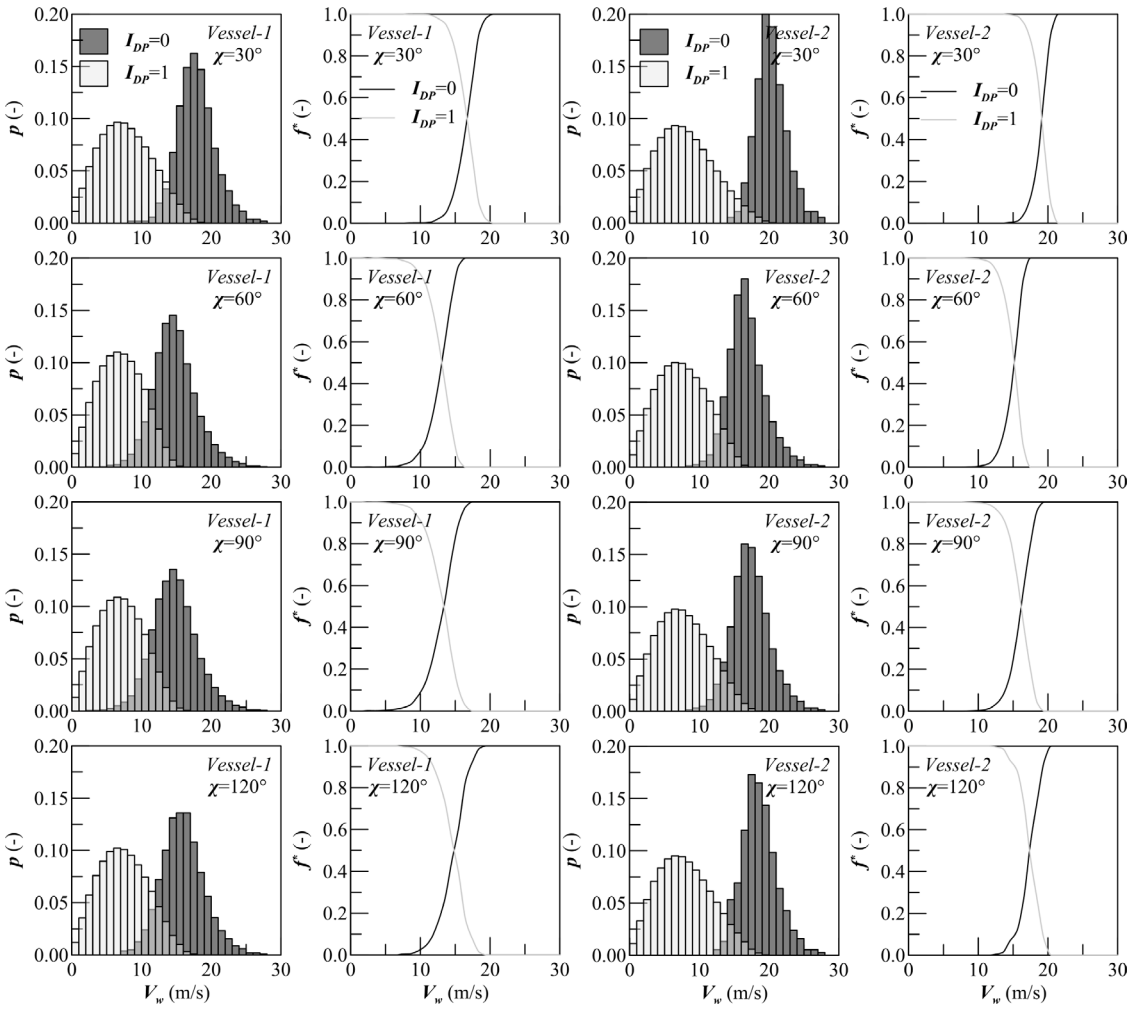

Fig. 16. Probabilities and relative frequencies of cases with $I_{DP} = 1$ and $I_{DP} = 0$ for *Vessel-1* and *Vessel-2* in Site B.

and DNV wind–wave correlations shown in Fig. 4 rather then with the IMCA one. The site-specific wind–wave correlation maximum wind limit is higher than the f^*=0.5 probabilistic curve for head and stern directions, but the limits are close within each other for beam headings (where the conventional site-specific limit is inside the band $0<f^*<1$). For *Vessel-2* the shape is comparable, and the differences between the limiting wind speed values are at most in the order of 3 m/s considering deterministic correlations. The conventional site-specific wind limits are higher than the probabilistic ones for both sites, also considering the band $0<f^*<1$.

It is noteworthy that the predicted "probabilistic capability plots" for the two reference vessels are different between Site A and Site B, in line with the OP_{DP} calculation presented in the previous sections. This is an improvement compared to the conventional capability plot provided by site-specific wind–wave correlations (Fig. 4), where the limiting $V_{w_{max}}$ was almost equal between the two see sites, especially for *Vessel-2*.

For the reference vessels used in this study, the V_w vector has been discretised in intervals of 1 m/s, starting from zero wind speed up to the maximum values of 30 m/s. The maximum of 30 m/s has been chosen to include the highest values obtained by sampling V_w from the marginal wind distribution for Site B, which is more severe then that for Site A as highlighted by OP_{DP} calculations.

It should be noted that the obtained probabilistic site-specific capability plots are fully comparable with the conventional one, as the assumption of collinearity of wind, wave and current loads is the same and also the current modelling is equal. However, even though the results in terms of capability plots are comparable, the new approach based on the probabilistic joint-distribution for wind and waves gives additional information on the effective operability of the DP system in a given area. Thus, the probabilistic method adds to a conventional site-specific prediction all the benefits already provided by the quasi-probabilistic scatter diagram approach and an enhanced definition of the limiting environmental conditions.

8. Final remarks

The modelling of environmental conditions influences the prediction of DP performances. The adoption of wind–wave correlations (deterministic or site-specific) implies the evaluation of DP performances by means of capability plots and additional quantities associated with the maximum sustainable wind at each encounter angle χ. The employment of $H_s - T_p$ joint distributions (or a scatter diagram) allows for the evaluation of operability of the DP system in a given sea area, which is not directly correlated to DP capability. The newly developed probabilistic method based on trivariate joint $V_w - H_s - T_p$ distributions overcome the disassociated evaluation of capability and operability, allowing for a joint prediction of the two aspects within the same calculation process.

To summarise, the following options can be identified for the quasi-static assessment of DP performances on the base of different modelling for environmental conditions:

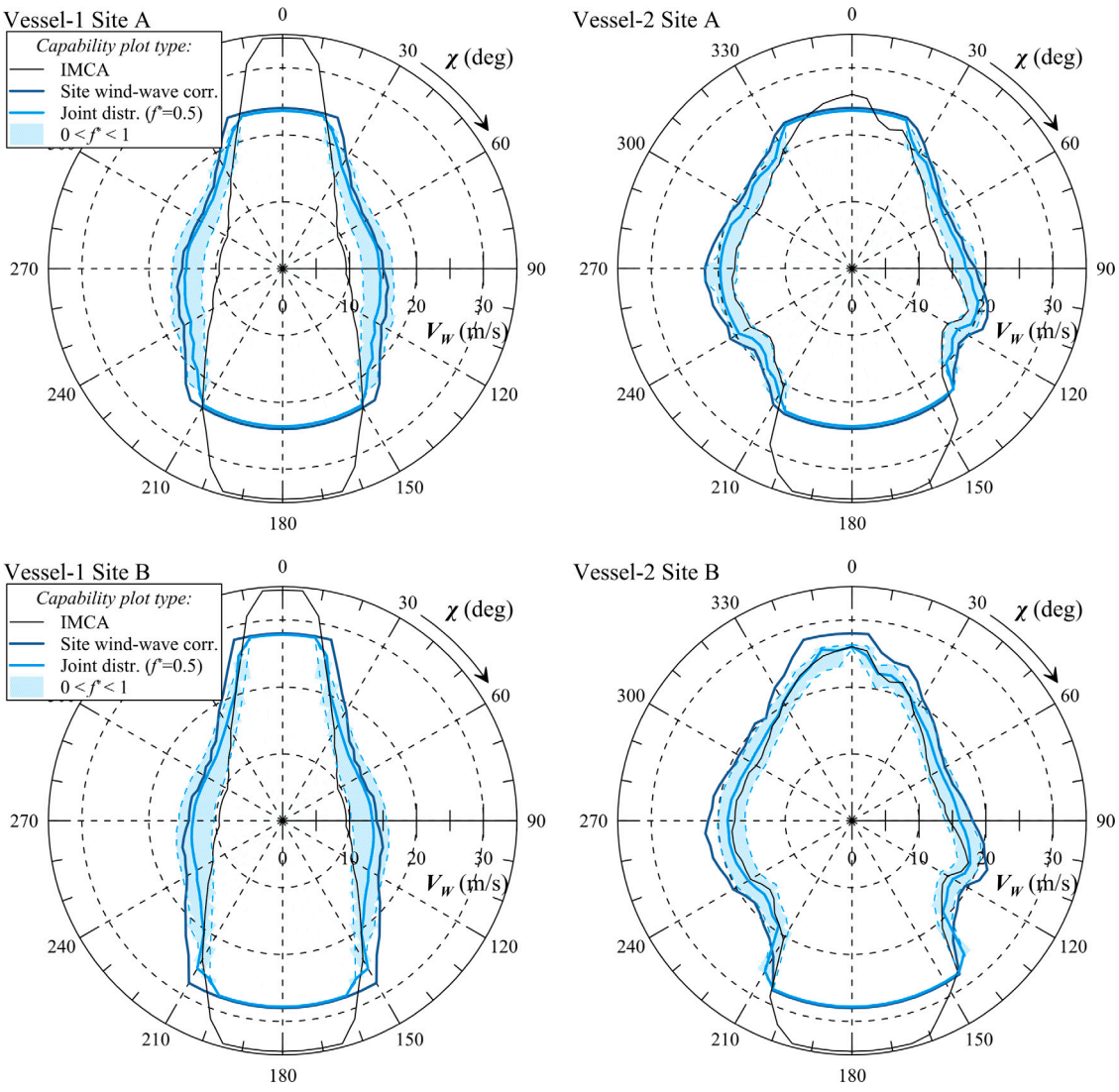

Fig. 17. DP capability plots according to IMCA standards, site-specific wind–wave correlations and joint-distribution for *Vessel-1* (*left*) and *Vessel-2* (*right*).

1. *Deterministic DP capability*: standard predictions using prescribed deterministic wind–wave correlations. The calculations determine the DP capability plot for the vessel according to different standards, as IMCA (IMCA, 2000) or DNV Level-1 and Level-2 (DNV, 2021) methods.
2. *Site-specific DP capability*: alternative method to determine DP capability employing site-specific wind–wave correlations instead of deterministic ones. An example of standard for these predictions is the DNV Level-2-site (DNV, 2021).
3. *Scatter diagram approach*: quasi-probabilistic method employing a joint distribution or the scatter diagram for the modelling of wave environment coupled with a PM correlation to determine wind speed. The method does not evaluate a capability plot but predicts the operability of the system for a given site.
4. *Probabilistic approach*: fully probabilistic method for the determination of site-specific wind and wave characteristics with trivariate joint distributions. The method is capable to evaluate DP operability with higher accuracy than the scatter diagram approach. Furthermore, the method provides also a capability plot to comply with site-specific conventional predictions.

The probabilistic approach allows for determining both capability and operability of the DP system for a given sea area, by providing a more detailed and comprehensive overview of DP system behaviour compared to the conventional site-specific prediction and scatter diagram approach.

As a last remark, as the probabilistic methods is an extension of the scatter diagram approach, the new method can be suitable to perform combined station keeping and seakeeping predictions (Mauro and Nabergoj, 2015b). Studies performed on the scatter diagram approach (Mauro and Nabergoj, 2020; Mauro et al., 2021), highlighted that imposing appropriate criteria to ship motions/accelerations in critical locations onboard it is possible to evaluate not only the operability of the system but also of the whole operation. This, in theory, applies also to the probabilistic method, inheriting all the improvements highlighted above. Such consideration further stress the capabilities and future developments of the newly proposed probabilistic process.

9. Conclusions

The adoption of probabilistic joint-distributions necessitates the implementation of a sampling process to evaluate the wind and waves parameters, adopting a numerical integration based on a Monte Carlo process to determine the DP operability. The present paper compares the performances of a conventional Monte Carlo process with a more convenient Quasi-Monte Carlo sampling based on Sobol sequences. Detailed analysis on two reference vessels (one Offshore Supply vessel and a Pipe-Lay vessel) in two different sea areas highlights the benefit

of the Quasi-Monte Carlo method on the reduction of cases needed to evaluate operability. As an additional output, the probabilistic method produces a limiting wind speed environment, defining a site-specific capability plot comparable with conventional predictions, which is of easier interpretation for offshore operators.

The proposed method is also suitable to perform combined predictions with motion/acceleration limits of the vessel. This may lead on future studies on the evaluation of an effective downtime period for a specific offshore operation, including transitions between stationing in operation, standby and survival during storm.

Furthermore, the same probabilistic approach can be extended to time-domain DP simulations, where the benefits in terms of accuracy of final results will be higher than calculations performed with quasi-static methods, but with a significantly increased calculation time. The environmental modelling could be further improved by including the current speed in the probabilistic joint-distribution modelling, supposing to dispose of the sufficient amount of data to fit a suitable distribution. Finally, the newly proposed probabilistic method increases the reliability of the environmental modelling for DP predictions, which is a significant improvement for the practical engineering applications of the offshore industry.

CRediT authorship contribution statement

Francesco Mauro: Conceptualization, Methodology, Software, Investigation, Writing – original draft, Writing – revised paper. **Radoslav Nabergoj:** Conceptualization, Writing – revised paper, Supervision.

Declaration of competing interest

The authors declare that they have no known competing financial interests or personal relationships that could have appeared to influence the work reported in this paper.

Data availability

Data will be made available on request.

Acknowledgement

The support of the NASDIS PDS d.o.o. (Slovenia) for the availability of model test data is acknowledged.

References

Aalberts, A., Kuipers, R., van Walree, F., Jansen, R., 1995. Developements in dynamic positioning systems for offshore stationkeeping and offloading. In: ISOPE Conference.

ABS, 2014. Guide for dynamic positioning systems. Technical Report, American Bureau of Shipping.

Arditti, F., Cozijn, H., van Daalen, E., Tannuri, E., 2019. Robust thrust allocation algorithm considering hydrodynamic interactions and actuator physical limitations. J. Mar. Sci. Technol. 24 (4), 1057–1070.

Arditti, F., Souza, F., Martins, T., Tannuri, E., 2015. Thrust allocation algorithm with efficiency function dependent on the azimuth angle of the actuators. Ocean Eng. 105 (1), 206–216.

Aydin, C., Ünal, U., Sariöz, K., 2022. Computation of environmental loads towards an accurate dynamic positioning capability analysis. Ocean Eng. 243, 110201.

Balchen, J., Jenssen, N., Saelid, S., 1976. Dynamic positioning using Kalman filtering and optimal control theory. In: IFAC/IFIP Symposium on the Automation in Offshore Oil Field Operation.

Bradley, P., Fox, B., 1988. Algorithm 659: implementing Sobol's quasi random sequence generator. ACM Trans. Math. Software 14 (1), 88–100.

BV, 2021. Rules for the classification of steel ships, part e. Technical Report, Bureau Veritas.

DNV, 2011. Rules for classification of ships. Technical Report, Det Norske Veritas.

DNV, 2014. DNV RP C205 environmental conditions and environmental loads. Technical Report, Det Norske Veritas.

DNV, 2021. DNV-ST-0111 assessment of station keeping capability of dynamic positioning vessels. Technical Report, Det Norske Veritas, Edition December 2021.

Hammersley, J., Handscomb, D., 1964. Monte Carlo Methods. Methuen & co. LTD.

Haver, S., 1980. Analysis of uncertainties related to the stohastic modelling of ocean waves. (Ph.D. thesis). Norvegian Institute of Technology, Trondheim, Norway.

Hogben, N., Dacunha, N., Olliver, G., 1986. Global Wave Statistics. British Maritime Technology Limited.

IMCA, 2000. IMCA M 140 Rev. I specification for DP capability plots. Technical Report, The International Marine Contractors Association.

Johannessen, K., Meling, T., Haver, S., 2001. Joint distribution for wind and waves in the north sea. In: Proceedings of ISOPE 2001. Stavanger, Norway.

Kumar, S., 2020. Dynamic Positioning for Engineers. CRC Press.

Levitan, Y., Markovich, N., Rozin, S., Sobol, I., 1988. On quasi-random sequences for numerical calculations. USSR Comput. Math. Math. Phys. 28 (5), 755–759.

Li, L., Gao, Z., Moan, T., 2013. Joint environmental data at five european offshore sites for design of combined wind and wave energy devices. In: Proceedings of the ASME 2013 32nd International Conference on Ocean, Offshore and Artic Engineering OMAE 2013. Nantes, France.

LR, 2021. Rules and regulations for the classification of ships, chapter 4. Technical Report, Lloyds Register, Edition July 2021.

Martelli, M., Faggioni, N., Donnarumma, S., 2022. A time-domain methodology to assess the dynamic positioning performances. Ocean Eng. 247, 110668.

Mauro, F., 2022. A flexible method for the initial prediction of tugs escort capability. Ocean Eng. 246, 110585.

Mauro, F., Benci, A., Ferrari, V., Della Valentina, E., 2021. Dynamic positioning analysis and comfort assessment for the early design stage of large yachts. Int. Shipbuild. Prog. 68 (1–2), 33–60.

Mauro, F., Gaudiano, F., 2018. Station-keeping calculations in early design stage: Two possible approaches. In: Proceedings of NAV 2018 Conference.

Mauro, F., Nabergoj, R., 2015a. Smart thrust allocation procedures in early design stage dynamic positioning predictions. In: Proceedings of the 18th International Conference of Ship and Shipping Research NAV 2015.

Mauro, F., Nabergoj, R., 2015b. Integrated station-keeping and seakeeping predictions. In: Towards Green Marine Technology and Transport. pp. 127–134.

Mauro, F., Nabergoj, R., 2016. Advantages and disadvantages of thruster allocation procedures in preliminary dynamic positioning predictions. Ocean Eng. 123, 96–102.

Mauro, F., Nabergoj, R., 2020. A global operability index for an offshore vessel. In: Proceedings of the ASME 2020 39th International Conference on Ocean, Offshore and Arctic Engineering OMAE 2020. Fort Lauderdale, FL, USA.

Mauro, F., Prpić-Oršić, J., 2020. Determination of a DP operability index for an offshore vessel in early design stage. Ocean Eng. 195, 106764.

Niederreiter, H., 1987. Point sets and sequencies with small discrepancy. Monatshefte Für Mathematik 104, 273–337.

Niederreiter, H., 1992. Random Number Generation and Quasi-Monte Carlo Methods. S.I.A.M., Philadelphia, PA.

Prpić-Oršić, J., Valčić, M., 2020. Derivative free optimal thrust allocation in ship dynamic positioning based on direct search algorithms. TransNav 14 (2), 309–314.

Smogeli, O., Trong, N., Borhaug, B., Pivano, L., 2013. The next level DP capability analysis. In: Dynamic Positioning Conference.

Sobol, I., Asotky, D., Krenin, A., Kucherenko, S., 2011. Construction and comparison of high-dimensional sobol'generators. Wilmott J. 64–79.

Wang, I., Yang, J., Xu, S., 2018. Dynamic positioning capability analysis for marine vessels based on dpcap polar program. China Ocean Eng. 32 (1), 90–98.